Pegah Khanjani

CELLULOSE-BASED SUPERHYDROPHOBIC SURFACES & DYNAMICS OF COUPLED CHEMICAL SYSTEMS

Thesis submitted for official examination for the degree of licentiate in technology

Espoo, April 28th 2015

Acknowledgements

The research reported in this thesis has been carried out firstly in molecular material group which its name was recently modified to the soft matter and wetting group, Department of Applied Physics at the Aalto University. I am grateful to my supervisor and thesis supervisor, Professor Robin Ras and Professor Mauri Kostiainen, for providing the good research facilities and for their support and helping me to grow more independent and flexible in adjusting to new projects and new people.

I would like to thank Professor Herbert Sixta for his valuable time for examining my thesis. It gives me great pleasure in expressing my gratitude to Professor Olli Ikkala and all those people who have supported me and had their contributions in making this thesis possible. Moreover, I thank Professor Janne Ruokolainen for the opportunity to work with electron microscopy and especially the scanning electron microscopes at the Nanomicroscopy Center. Special thanks to Nonappa, Maja, Johanna, and Henna for practical guidance and their critical suggestions have always been very helpful in improving my skills throughout the first project. I gratefully thank Taneli and Panu for implementing XRD measurement and their useful comments.

Finally, I would like to compliment my husband, Ali Akbari for his love and constructive discussions during this work and my studies, and for encouraging me to always attempt for better. I also express gratitude to my families and my friends for support and for fulfilling my free time with fun and laughter.

Aalto University
School of Science

Abstract of Licentiate Thesis

Author

Pegah Khanjani

Title of Thesis

Cellulose-based superhydrophobic surfaces & Dynamics of coupled chemical systems

Abstract

Superhydrophobic surfaces can be found in plants, insects, and bird feathers[1]. Inspired by natural superhydrophobic surfaces, researchers have recently developed and constructed superhydrophobic surfaces in a variety of smart and simple ways[2,3,4]. The hydrophilic property of cellulose nanocrystals (CNCs) was modified by the esterification of CNCs with low surface energy chemicals of 2H,2H,3H,3H-Perfluorononanoyl chloride and 2H,2H,3H,3H-Perfluoroundecanoyl chloride, respectively. A stable suspension of nanospherical fluorinated cellulose ester was obtained by using the nanoprecipitation technique. The resulting nanostructured fluorinated cellulose esters was simply coated on a paper surface to gain a superhydrophobic paper surface characterized by a contact angle over 150º. The superhydrophobic paper remained stable even at a high temperature, showing no signs of melting or damage. The hydrophobized paper was characterized by nuclear magnetic resonance (NMR), infrared spectroscopy (IR), and static contact angle (CA) measurement. Further, we investigated the size, shape, and amorphicity of nanostructured fluorinated cellulose esters by light scattering (DLS), scanning electron microscopy (SEM), and X-ray diffraction (XRD) measurements. The development of economically and ecologically viable strategies for the superhydrophobization of surfaces for the introduction of a self-cleaning property offers a vast variety of interesting applications. Examples include packaging materials, textiles, outdoor clothing, and microfluidic devices.

The dynamics of oscillation in chemical reactions as a research field has grown dramatically over the past 50 years and produced thousands of studies on about 70 known chemical oscillators. Oscillating chemical reactions find many applications in physics, biology, physiology, geology, and medicine[64]. The dynamics of the bromate-sulfite-ferrocyanide (BSF) reaction is studied in a well-mixed open chemical reactor, called a continuous stirred tank reactor (CSTR). A CSTR system can be used to investigate the dynamics of out-of-equilibrium chemical processes, such as oscillation, bistability, and chaos[65]. This BSF reaction exhibits periodic oscillation as a function of $[H^+]$, called pH oscillation. The reaction was carried out at 25ºC, and the flow rate was 1 and 2 mL/min. The pH oscillation occurs only in a specific range of flow rates. Here, we show regular pH oscillation in a BSF system by utilizing different concentrations under a nitrogen atmosphere. Such a pH oscillator system can be coupled or probed with pH-sensitive systems, and it helps to understand new mechanisms may arise by periodic behavior[66].

Research field	**Key words**
Engineering Physics	Superhydrophobicity, Perfluorinated cellulose esters, pH oscillation, BSF system.
Supervising professor	**Pages**
Professor Robin Ras	59
Thesis advisor	**Language**
Professor Mauri Kostiainen	English
Thesis examiner	**Date**
Professor Herbert Sixta	28.4.2015

☒ **The thesis can be read at https://aaltodoc.aalto.fi/handle/123456789/27**

Cellulose-based superhydrophobic surfaces

1. Introduction

1.1. Structure and reactivity of cellulose

Cellulose is the most abundant polymer in nature. It is a linear and fairly rigid homopolymer consisting of D-anhydroglucopyranose unit (AGU). A deep understanding of the structural properties of cellulose requires studying the effect of different substituents on the physical and chemical properties of cellulose and its derivatives. Anselm Payen was the first to find the chemical composition of cellulose, which is presented by the elemental formula $(C_6H_{10}O_5)_n$[5]. In the late 1920, Haworth proposed a chain-like macromolecular structure after Hermann Staudinger proved the highly polymerized nature of cellulose. The repeat unit consists of two AGU rings ($(C_6H_{10}O_5)_n$; n= 10000 to 15000, where *n* depends on the cellulose source material) that are linked together through a β-(1→4) glycosidic bond. Figure 1 shows the β-(1→4 linkage) glycosidic bond formed between the C1 of one glucose ring and the C4 of the connecting ring. The *n* shows the number of AGU units linked together and it is commonly known as the "degree of polymerization" (DP). In solid state, AGU has three hydroxyl (OH) groups at the C-2, C-3 and C-6 positions. The terminal groups at the either end of the cellulose are different from each other. The C-1 hydroxyl at one end of the molecule is a hemiacetal group with reducing activity and creates from the formation of the pyranose ring via an intramolecular hemiacetal reaction. In contrast, the C-4 hydroxyl group at the other end of the molecule is an alcoholic hydroxyl group and denotes the non-reducing end[6] (Figure 1). These hydroxyl groups, one primary and two secondary, can be substituted with different functional groups by esterification, etherification, fluorination, silylation, amination, carbanilation or grafting the polymer of cellulose surface. It is known from infrared spectroscopy (IR), X-ray crystallography and nuclear magnetic resonance (NMR) that the AGU ring exists in the pyranose ring conformation and that this adopts the $^4C_1$-chair formation which constitutes the lowest energy conformation for D-glucopyranose[7].

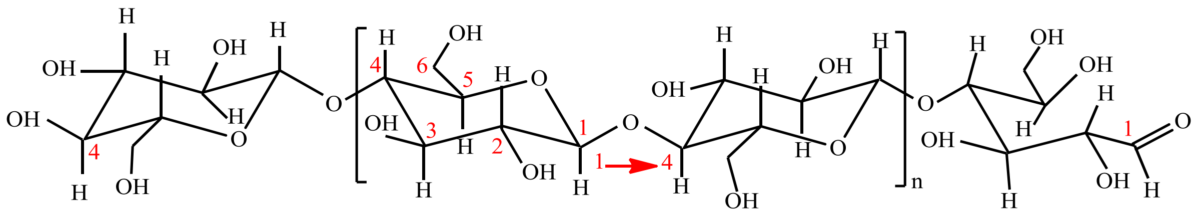

Figure 1. Molecular structure of cellulose representing the repeating unit that shows reducing (right) and non-reducing (left) end-group and also β-(1→4 linkage).

There are two possibilities for the hydroxyl groups in the cellulose molecule to form hydrogen bond. The interaction between hydroxyl groups in the same molecule creates intramolecular hydrogen bonding but when the interaction is between two hydroxyl groups in neighboring cellulose molecules, then it forms intermolecular hydrogen bonding. The two intramolecular hydrogen bonds are formed between the hydroxyl groups on C-3 and the endocyclic oxygen (O5) and between the C2-OH and the C6-OH groups. Intramolecular hydrogen bond is the main cause of the high stiffness and rigidity of the cellulose molecule that gives cellulose high viscosity in solution, its high tendency to crystallize, and its ability to form fibrillar strands. The intermolecular hydrogen bonds are made from the bonds between the C3-OH and C6-OH (Figure 2).

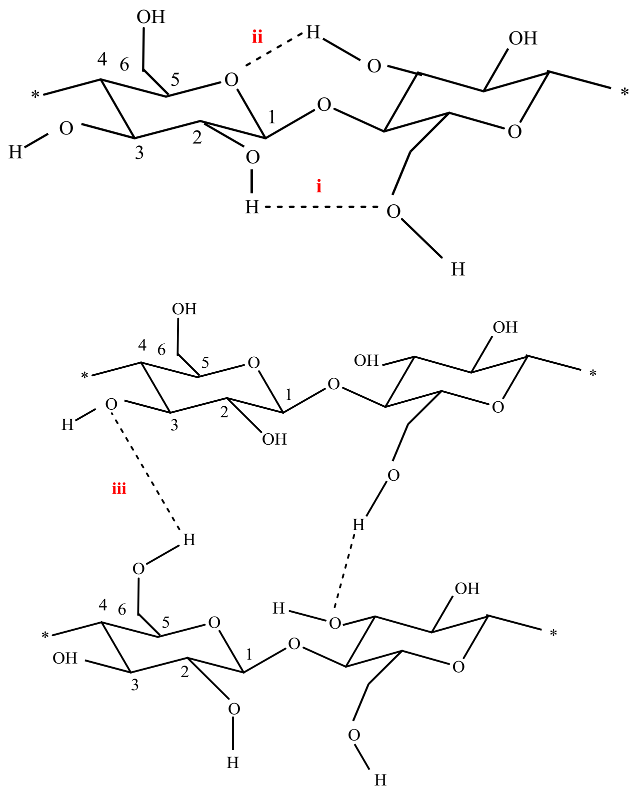

Figure 2. Cellulose structures showing the intramolecular hydrogen bonding between C2-OH and C6-OH (i), and C3-OH with endocyclic oxygen (ii); and the intermolecular hydrogen bonding between C3-OH and C6-OH (iii) (supramolecular structure)[8].

Cellulose is insoluble in common organic solvents and in water[6]. This is due to the both extensive intra- and intermolecular hydrogen bonding and also hydrophobic interactions. The axial direction of the AGU ring is hydrophobic since the hydrogen atoms of carbon-hydrogen bonds are located on the axial position of ring[9]. Breaking the hydrogen bonding network increases the solubility of cellulose in polar and non-polar solvents.

The properties of cellulose depend on its molecular, supramolecular and morphological structure.

1.2. Supramolecular structure of cellulose

Cellulose chains have the tendency to aggregate and form a parallel arrangement of crystallites and crystallite strands. The ability of hydroxyl groups of cellulose to form secondary valence bonds with one other is the main reason for strong tendency of cellulose to organize in parallel arrays of crystallites[10].

Nishikawa and Ono discovered the supramolecular structure of cellulose by studying the well-defined X-ray diffraction patterns. This led to the conclusion that individual cellulose molecules tend to arrange themselves in a highly organized way leading to a “paracrystalline” state. Based on “micellar structure” concept, Naegeli and Schwenderner proposed in 1865 that the natural reticulum substrates, such as cellulose which built from particles of colloidal dimensions. These colloidal particles are called “micelles” and they are held together by glue-like materials. Based on these assumptions and theories of Staudinger on the macromolecular structure, scientist developed the “fringe-micellar” structure concept (Figure 3A). According to this structure model, polymer chain alignment form crystalline domains (“micelles” or “crystallites”). The supramolecular structure consists of two regions: low order “amorphous” and highly order “crystalline”[11]. The crystallites are embedded in an amorphous matrix due to the two phase network.

a b

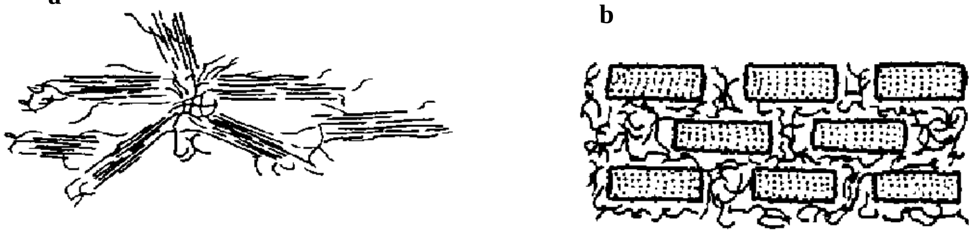

Figure 3. a) Fringe-micellar model and b) micellar structure model mixed with amorphous material[6].

According to the Figure 3B, the latticework represents the highly ordered crystalline region, while the residual part represents the low ordered amorphous regions. The degree of crystallinity can be measured by different X-ray techniques such as powder X-ray diffraction (XRD), and other means such as solid state NMR spectroscopy.

There are several polymorphs of crystalline cellulose (I, II, III, IV). Each has been broadly studied[12]. Cellulose I is the crystalline cellulose that is naturally produced by a variety of organism like plants, algae, bacteria, etc. and it is sometimes referred to as "natural" cellulose. Its structure is thermodynamically metastable and can be converted to the cellulose II or III[12]. The cellulose II crystal structure is the thermodynamically most stable one and can be produced by two processes of regeneration (solubilization and recrystallization) and mercerization (aqueous sodium hydroxide treatments)[13]. Crystalline cellulose I is a mixture of two polymorphs, comprising a triclinic (Iα) and a monoclinic (Iβ) structure, which are shown in Figure 4. Since there is a difference between Iα and Iβ unit-cell parameters, small shift in the cellulose chains in one arrangement along the chain axis can be seen (Figure 4a). Three lattice planes with approximate d- spacings of 0.39 nm, 0.53 nm, and 0.61 nm are shared and correspond to Iα lattice planes $(110)_t$, $(010)_t$, and $(100)_t$, and Iβ lattice planes $(200)_m$. $(110)_m$, and $(1\bar{1}0)_m$, respectively. There is a relative displacement of c/4 between each subsequent hydrogen-bonded plane for Iα, while for Iβ the displacement alternates between +c/4 and − c/4. For both Iα and Iβ unit cells the cellulose chains are arranged in a "parallel up" configuration in which all the cellulose chains are arranged such that the 1→4 link points in the positive c-axis direction of their respective crystalline unit. In contrast, "antiparallel" describes alternating stacking of the cellulose chains in the 1→4 link directionality between different hydrogen bonding planes.

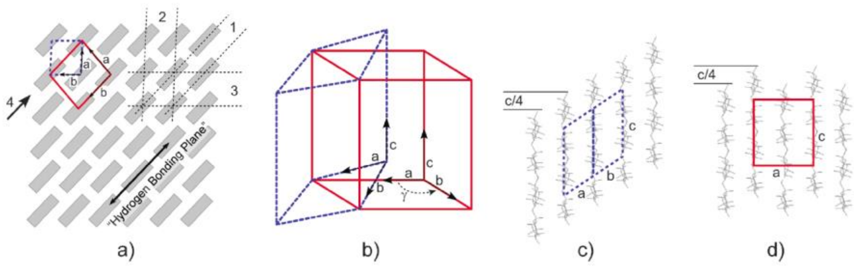

Figure 4. Schematic of the unit cells for cellulose Iα (triclinic, dashed line) and Iβ (monoclinic, solid line). (a) projection along the chain direction with the Iα and Iβ unit cells superimposed on the cellulose I crystal lattice[14] *showing the parallelogram shape of both unit cells when looking down the c-axis. The corresponding lattice planes for 1, 2, and 3, are (110)t, (010)t, and (100)t for Iα and (200)m, (110)m, and (1$\bar{1}$0)m for Iβ. (b) relative configuration of Iα with respect to Iβ unit cell*[15]*, and the displacement of the hydrogen bonding sheets for (c) Iα of +c/4, and for (d) Iβ alternating +c/4 and −c/4*[13].

1.2.1. Morphological structure of cellulose

The morphological structure of cellulose contains a well-organized architecture of fibrillar elements. Information on cellulose morphology is acquired mainly by electron microscopic techniques (scanning and transmission electron microscopy), but also light microscopy exclusively employed in the first part of this century, is still a necessary tool in the investigation of the gross morphology. An elementary fibril is the smallest morphological unit with variable size depending on the source of cellulose. A uniform and a non-uniform elementary fibril have 3.5 and 3-20 nm in diameter, respectively. The microfibril is the lowest well-defined morphological entity, although it consists of non-uniform subunits. The microfibrils aggregate to larger morphological entities with diameters in the range 10-50 nm, and significantly depending on the cellulose origin. The length of the microfibrils can reach micrometers.

Micro- and macrofibrils contain units of the cellulose fiber cell-wall architecture. This cell-wall morphology is characterized by layers differing in fibril texture, as shown schematically in Figure 5 for a cotton fiber and a delignified spruce pulp fiber. Despite the different origin and function of these fiber cells, some general similarities of morphological architecture can be recognized. Both fibers consist of different layers with the fibril position giving different densities and textures. In the outer layer, the so-called primary wall (P) fibrils of about 10 nm in diameter are positioned crosswise to a layer of about 50 nm thickness. This crosswise positioning possibly impedes a swelling of the inner secondary wall. The secondary wall (S) consists of two layers Sl and S2. The thickness of the Sl layer is, in the case of cotton, about 100 nm, in the case of a spruce pulp fiber, about 300 nm. The fibrils are aligned parallel and densely packed in a flat helix, the direction of which may be opposite in subsequent Sl layers. The Sl layer can strongly impede swelling of the S2 layer beneath it, the thickness of which amounts to several µm and thus contains most of the cellulose mass. The fibrils are well aligned in a helix. In the cotton fiber, a layered structure of S2 exists due to density fluctuations during growth, with an average distance of 100-200 nm, which becomes visible after suitable swelling treatment. The inner layer closest to the fiber lumen, i.e. the tertiary layer (T) in the case of wood fibers and the S3 layer in the case of cotton, is comparably thin and has the fibrils aligned in a flat helix[16].

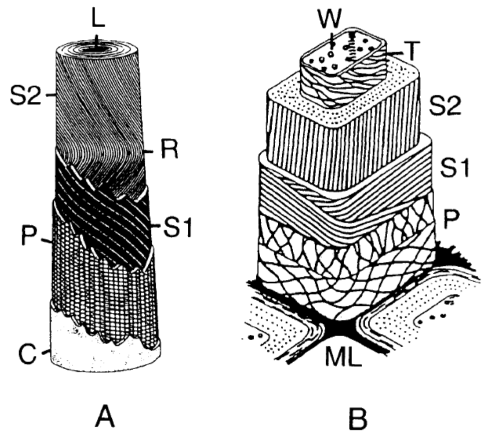

Figure 5. Scheme of the 'morphological architecture' of a cotton fiber (A) and a delignified spruce wood fiber (B); C-cuticle (rich in pectins and waxes), L-lumen, ML-middle lamella (mainly lignin), P-primary wall, R-reversal of the fibril spiral, Si-secondary wall ('winding layer'), S2-secondary wall (main body), T-tertiary wall, W-wart layer[16].

For the determination of the dimension of fibrous cellulose substrates there are three methods available: 1) heterogeneous hydrolytic degradation, 2) electron microscope imaging, and 3) X-ray wide and small angle diffraction. In the current study we did X-ray diffraction measurement in order to investigate the crystalline structure of the synthesized fluorinated cellulose ester.

1.3. Isolation of cellulose particles

The isolation process of cellulose from cellulose source materials comprises two stages. The first stage is purification and homogenization pretreatment of the source material. The specific treatment depends on the cellulose source material (like wood, plants, tunicate, algal, and bacterial cellulose source) and to a lesser degree on the desired morphology of the starting cellulose particle for the second stage treatments[17]. The second step constitutes the separation of these “purified” cellulose material into microfibrillar and/or crystalline components. Isolation of cellulose can be achieved by different measures such as *mechanical treatment, acid hydrolysis, and enzymatic hydrolysis*[18]. These methods can be carried out separately, however in practice these methods are used in sequence for obtaining the desired morphology.

Acid hydrolysis method is for extracting the crystalline particles from the cellulose material sources.
This process removes the amorphous regions within the cellulose microfibrils. Typically, sulfuric acid is used since it introduces a negative charge onto the surface of particles through sulfation, leading to more stable suspensions but other acids like hydrochloric and maleic acid can also be used. If hydrolysis is carried out using hydrochloric acid instead of sulfuric acid, the cellulose whisker dispersion becomes more unstable and there is a tendency to jellify, which is not desirable for most end applications[19]. Finally, the mixture has to be separated by centrifugation or filtration and washing/rising step by dialysis against deionized water to remove the remaining acid or neutralized salt.

In our study cellulose nanocrystals (CNCs) were prepared by the sulfuric acid hydrolysis, which introduces sulfate groups on the crystallite surface. Charged sulfate groups enable stable dispersions due to electrostatic repulsion, suppressing the inherent tendency of aggregation[20].

1.4. Cellulose based materials

Here, the main cellulose-based materials based on different cellulose sources and also various cellulose extraction methods are briefly described. The most abundant cellulose-based material is wood and to a lesser extent annual plants[13]. These individual wood or plant cells that are 10's of micron in diameter and millimeters in length. They have a high percentage of cellulose and relatively low crystallinity (43–65%). *Microcrystalline cellulose (MCC)* is prepared by acid hydrolysis of hemicellulose-lean pulp (dissolving pulp), back-neutralization with alkali and then spray-coating. The resulting particles are approximately 10–50 μm in diameter. Usually the MCC aggregates are broken to smaller rode-like particles with 1–10 μm in length for the use in composites. Another type of the cellulose particle is *Microfibrillated cellulose (MFC)* which is produced by mechanical treatment of wood and plant fiber pulps. Their dimensions in width and length are 10–100 nm and 0.5–10 μm, respectively. Nevertheless, they have a high aspect ratio and contain both amorphous and crystalline regions[13]. The dimensions of nanofibrillated *cellulose (NFC)* are smaller as compared to MFC, comprising a typical width and length of 4–20 nm and 500–2000 nm, respectively. The differentiation of NFC from MFC is based on the fibrillation process that produces finer particle diameter. Typical dimensions of CNCs prepared from filter paper are in the range of 5–8 nm in diameter and 50 to 500 nm in length. The rod-like or whisker shaped particles of CNCs contain a high aspect ratio and are highly crystalline (54–88%)[13].

Insufficient hydrolysis process leads to modify cellulose morphology since the amorphous region is not completely remove. However, acid hydrolysis can be improved by increasing the reaction time or increase the acidity, which results in more pronocunced depolymerization of the crystalline cellulose, thereby reducing the size of the particles. The largest aspect ratio of the CNC is *Tunicate cellulose nanocrystals*, which have height of almost 8 nm, a width of 20 nm, and a length of 100–4000 nm. Algae cellulose and bacterial cellulose particles are other types of cellulose particles which are extracted from the wall of various algae and bacteria, respectively.

2. Strategies of cellulose surface modification

The cellulose modification relies on surface functionality of hydroxyl groups. CNCs displays to main drawbacks. The first one is the high number of hydroxyl groups, which lead to strong hydrogen interactions between two nanocrystals and producing the gel-like structure. The second drawback is the high hydrophilicity of this material, which limits its uses in several applications such as in paper coating (increase of dewatering effect) or composites (tendency to form agglomerates in petro-chemical polymers). The most feasible solution to this is chemical surface modification to reduce the number of hydroxyl interactions and also to increase the compatibility with several matrices. Generally, the chemical modification of CNCs can be classified into two distinct groups: (1) Physical interaction or adsorption of molecules or macromolecules onto their surface, and (2) Chemical approach to achieve covalent bonds between cellulose substrate and the grafting agents.

The aim of this chapter is to briefly highlight some of the chemical pretreatment methods to prepare the CNCs and the functionalization of this material via the absorption and the chemical modification. The chemical pretreatment methods are used to introduce stable negative or positive electrostatic charges on the CNCs surface to obtain better dispersion. Finally, among of the chemical derivatization methods, acylation of cellulose at heterogeneous condition will be shortly discussed.

2.1. Functionalization via CNC synthesis

The surface chemistry of cellulose nanoparticles is primarily controlled by the extraction procedure used to prepare these nanoparticles from the native cellulosic substrates. Therefore this modification method is provided by the most common extraction methods, which CNCs represent one of two chemistries at the surface (Figure 6). As an example the CNCs can contain acid content at their surface. Cellulose sulfation can be carried out by sulfuric acid treatment when it forms sulfate ester on the CNCs surface. The sulfate content provides a high charge on the surface of the cellulose that leads to a stabilized nanocellulose dispersion. This method has been used for enriching sulfate groups on the crystal surface. Other less used methods have been presented as well, such as phosphoric acid and hydrobromic acid.

Fischer-Speier esterification is another method to obtain acetylated surface. Fibrillated CNC types are derived from different methods for surface modification and they show different surface chemistry. TEMPO-mediated oxidation is another common method. In this method uses the 2,2,6,6-Tetramethylpiperidine 1-oxyl (TEMPO) radical as a catalyst with a primary oxidant such as hypochlorite to selectively oxidize primary alcohol groups in the cellulose. In fact primary alcohol group of nanofibrillated cellulose oxidized into the carboxylic acid.

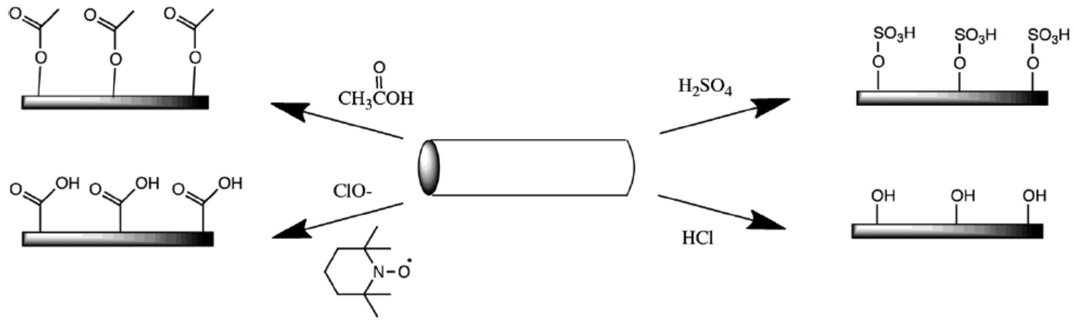

Figure 6. Specific surface chemistries provided by the most common extraction methods of cellulose nanoparticles: sulfuric acid treatment provides sulfate esters (top right), hydrochloric acid treatment provides hydroxyl (bottom right), acetic acid provides acetyl (top left), TEMPO mediated hypochlorite treatment provides carboxylic acid (bottom left)[13].

2.2. Functionalization via adsorption

The second modification procedure involves the adsorption of molecules from a gas, liquid, or dissolved solid to the surface of particles. Noncovalent surface modifications of CNCs are made via adsorption of surfactants. Using surfactants is useful to stabilize nanoparticles in nonpolar solvents. This approach has been introduced by Heux et al., who used surfactants consisting of the mono- and di-esters of phosphoric acid bearing alkylphenol tails. An anionic surfactant was also investigated by Bondeson et al. to enhance the dispersion of CNCs in poly (lactic acid) (PLA). Kim et al. [21] and Rojas et al.[22] used nonionic surfactant to disperse the CNCs in polystyrene-based composite fibers. A cationic surfactant dioctadecyldimethylammonium bromide was used to prepare a cellulose–surfactant complex that allowed transfer of the nanocrystal from the aqueous suspension to the hydrophobic solid substrate. Another common method via adsorptive modification is the electrostatic adsorption of macromolecules, which should bear both hydrophobic and hydrophilic moieties. This method is borrowed from the manufacture paper as it has long been known that cellulose is weakly charged and polyelectrolytes have been used as dry and wet strength additives, anti-static, and other uses. Functionalization via non-covalent interaction, where surfactants or polyelectrolytes are absorbed on the surface, can be often applied for improving the nanocellulose dispersibility or to control the assembly of individual fibrils into layered structures.

2.3. Functionalization via chemical modification

The last method of surface chemical modification is via derivatization or/and covalent attachment of molecules. Since cellulose has hydroxyl groups on its surface, there are techniques that react with alcohols like isocyanates, epoxides, acid halides, and acid anhydrides through chemical reactions. These reactions can be utilized to introduce a host of alternate surface chemistries such as amine, ammonium, alkyl, hydroxyalkyl, ester, acid, etc. Another modification resorts to TEMPO mediated oxidation of HCl derived nanocrystals to convert primary alcohol groups to carboxyl groups for better dispersibility. The formation of sulfate esters via the reaction of cellulosic OH-groups with sulfation agent acid introduces negative charges to the surface. Homogeneous sulfation of bagasse cellulose was studied in an ionic liquid 1-butyl-3-methylimidazolium chloride ([C_4mim]Cl) in order to obtain anticoagulation active cellulose sulfates[23]. Previous studies on the sulfation of cellulose have been carried out either in a heterogeneous system starting with an activated cellulose suspension, or a homogenous system starting with partially substituted cellulose derivatives in an aqueous solution[23]. A major problem with the heterogeneous system is the unequal accessibility between the OH groups in the amorphous regions and those in the crystalline regions, leading to inhomogeneous substitution. In contrast, DS values in homogeneous reactions are limited to the available hydroxyl groups at the reaction starts with substituted derivatives. Another modification example is polymer grafting, where a range of different polymers with various properties attach on the surface. Surfaces can also be silylated by using chloro- and alkoxy-silanes. There is a covalent linkage of the silanes to the cellulose surface[24].

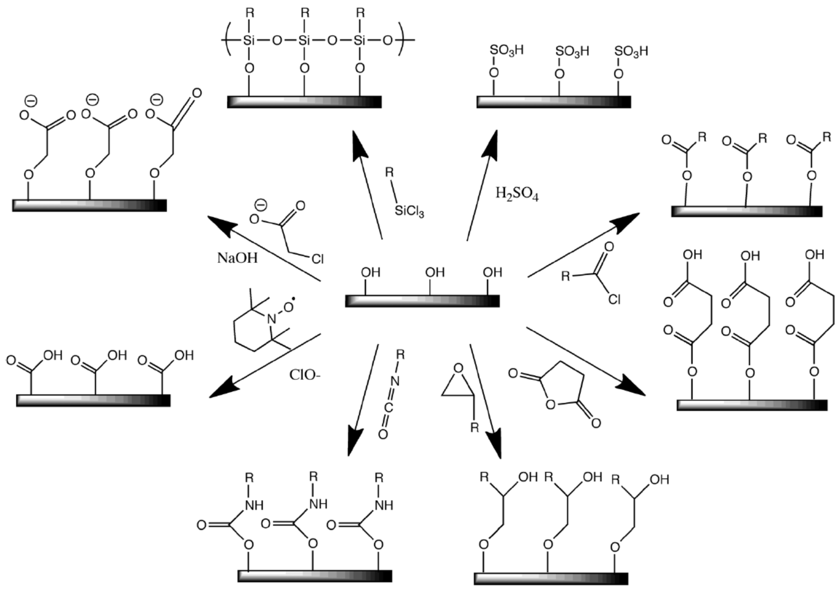

Figure 7.Common modification chemistries of CN surfaces: (clockwise from top-right) sulfuric acid treatment provides sulfate esters, carboxylic acid halides create ester linkages, acid anhydrides create ester linkages, epoxides create ether linkages, isocyanates create urethane linkages, TEMPO mediated hypochlorite oxidation creates carboxylic acids, halogenated acetic acids create carboxymethyl surfaces, an chlorosilanes create an oligomeric silylated layer[13].

In the present project the surface modification was achieved by esterification of perfluoroalkyl compounds with cellulose surface molecules to obtain super-hydrophobic nanoparticle cellulose esters. Esterification can be done under heterogeneous or homogenous reaction conditions. Since we have long chain aliphatic acid chloride, the synthesis was carried out under heterogeneous conditions.

2.3.1. Esterification of cellulose

As mentioned above, three hydroxyl groups in each glucose unit of the cellulose chain molecules are able to react with inorganic and organic acids or acid chlorides and anhydrides to form cellulose esters. Herein, I describe the heterogeneous acylation of cellulose.

2.3.1.1. Acylation with acid chlorides and anhydrides

The esterification can be done through homogenous reactions in ionic liquid or heterogeneous reactions in pyridine using fatty acid chlorides as acylating agents[25,6]. Conventional acylation is applied for the substitution of hydroxyl groups of cellulose with an acyl derivative. Herein, an overview on general different techniques and their specific potential is reported.

I. Acid-catalysed heterogeneous acylation

The most common acylation of polysaccharides is conducted with carboxylic acid anhydrides under heterogeneous conditions.

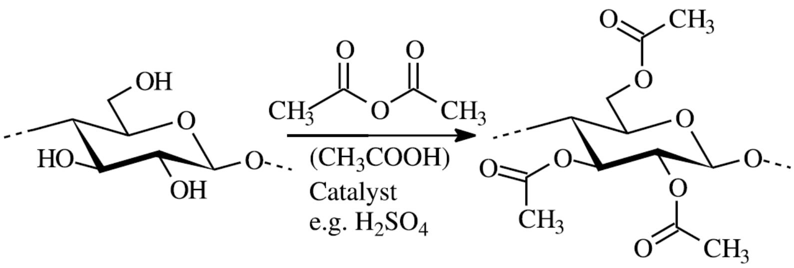

Figure 8. Conversion of cellulose with acetic anhydride/acetic acid[26].

As Figure 8 shows, cellulose acetate is produced by conversion of cellulose with the mixture of acetic acid and acetic anhydrides in the presence of sulfuric acid as a catalyst (up to 15% w/w). Acylation is improved via the formation of reactive mixed anhydrides, which is known as the “impeller” method (Figure 9). The carboxylic acids or their anhydrides are converted in situ to reactive mixtures of symmetric and mixed anhydrides. Chloroacetyl, methoxyacetyl- and, most important, trifluoroacetyl moieties are used as impellers[27]. They lead to modify polysaccharides. However, the behavior of impeller ester functions in the polysaccharide, i.e. trifluoroacetyl moieties are not found. Reactivity of cellulose esters is observed to decrease in the order acetic > propionic > butyric acid.

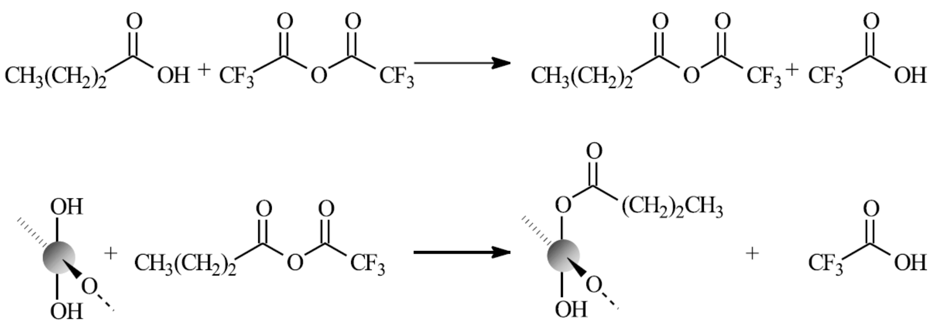

Figure 9. Acylation of polysaccharides via reactive mixed anhydrides (impeller method)[28].

The impeller method can be applied for the synthesis of starch acetates and cellulose benzoates with complete functionalization. The reaction will be completed if the polysaccharide dissolves in the reaction mixture (after about 75 min at 60 °C)[29].

II. Base-catalysed heterogeneous acylation

Esterification reaction with carboxylic acid anhydrides and acidic catalysis under acidic catalysis are associated with chain degradation. The side reaction is used to tune the DP of the products. Tertiary bases such as pyridine and triethylamine are commonly used to suppress the degradation. The base forms a semi-liquid mixture with polysaccharides and functions as the acylation catalyst. The triacetate of cellulose is obtained after long reaction times of 6 to 10 days at 60 °C. The same process can be done for starch as well, which leads to starch triacetates however by increased temperature to 100 °C, the reaction time can be reduced to 24 h. Another way for increasing the reactivity is the addition of 4-Dimethylaminopyridine, which increases the rate of the reaction by up to 10^4 times. The catalytic efficiency is probably due to the stabilization of the acylpyridinium ion, which plays an important role in the catalytic cycle. In the heterogeneous conversion of polysaccharides, usually pyridine is widely used for the preparation of fatty acid of polysaccharides. These esterification reactions lead to highly functionalized esters which are insoluble in nonpolar solvents (Figure 10).

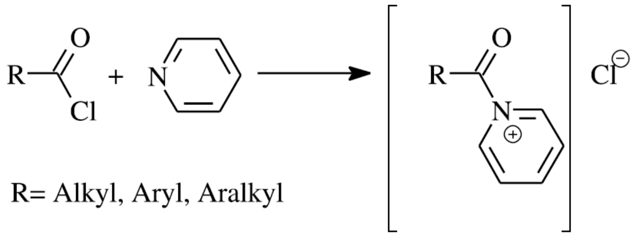

Figure 10. Acylium salt formed from an acid chloride and the tertiary base Py[28].

During the esterification procedure, the acylium salt from an acid chloride and the tertiary base pyridine produce a product which is mostly brown because of side reactions and production of byproducts. Such a brown product was observed in our investigation for both esterification reactions with pyridine and different acid chlorides of 2H,2H,3H,3H-perfluorononanoyl chloride and 2H,2H,3H,3H-perfluoroundecanoyl chloride, respectively. These side reactions are mainly polycondensation and the products can be purified by washing with ethanol, soxhlet extraction with ethanol or precipitation from chloroform in ethanol. The formation of 2-methyl-3-oxo-pentanoyl groups can lead to propionylation through the mechanism shown in Figure 11, which have low DS values[30].

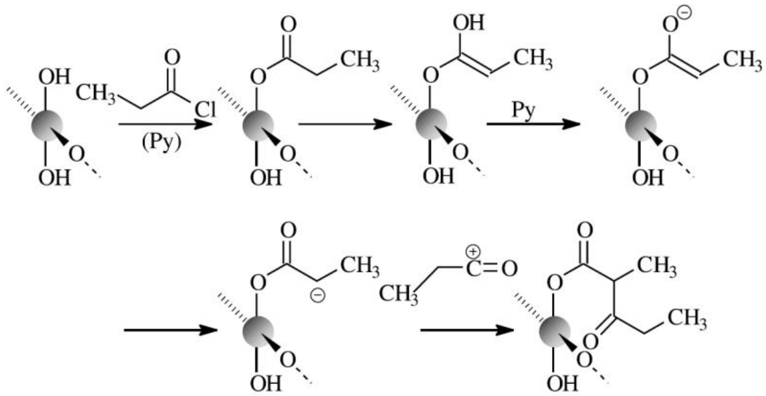

Figure 11. Reaction mechanism for the formation of 2-methyl-3-oxo-pentanoyl groups during the propionylation of polysaccharides with propionyl chloride in Py[31].

The extent of side reactions of esterification of starch, dextran and cellulose with acid chlorides can be reduced by carrying out the reaction in DMF or DMAs as slurry medium or in homogeneous cellulose solution in DMAc/LiCl without using any base. The DS value diminishes by the utilization of an excess of base, according to the Table 1, which shows the relevant results of acylation of cellulose in pyridine with propionyl chloride[30]. Another improvement method for increasing the reactivity of acylation is using DMP to increases the reactivity of acylation systems.

Table 1. Acylation of cellulose in Py with propionyl chloride at 100 °C for 4 h (adapted from[30])

Molar ratio AGU	Py	Propionyl chloride	Product DS	Solubility in $Cl_2CHCHCl_2$
1	27.6	4.5	1.86	–
1	18.9	6.0	2.66	+
1	12.0	6.0	2.80	+
1	12.0	4.5	2.70	+
1	9.9	9.0	2.13	+
1	7.5	6.0	2.89	+
1	6.0	4.5	2.81	+
1	4.8	4.5	2.86	+
1	3.0	4.5	2.89	+
1	1.5	4.5	2.84	+

Acylation is best to perform in a mixture of base and a diluent. Table 2 gives an overview of results for the cellulose propionylation with different diluents and bases, showing that the use of pyridine in combination of 1,4-dioxane, chlorobenzene, and toluene. In the present study the perfluorinated cellulose esters were obtained by applying the pyridine and toluene mixture.

Table 2. Cellulose propionylation with different diluents and tertiary amine using 1.5 mol propionyl chloride/mol AGU at 100 °C[28].

Conditions Medium	Base	Time (h)	Product DS
Dioxane	Py	4	2.81
Dioxane	β-Picoline	4	2.70
Dioxane	Quinoline	4	2.18
Dioxane	Dimethylaniline	48	1.57
Dioxane	γ-Picoline	24	Negligible
Chlorobenzene	Py	4	2.86
Toluene	Py	4	2.30
Tetrachloroethane	Py	24	2.23
Ethyl propionate	Py	5	2.16
Isophorone	Py	4	1.89
Ethylene formal	Py	22	0.34
Propionic acid	Py	5	0.20
Dibutyl ether	Py	22	Negligible

The heterogeneous acylation of cellulose is a well-established and reproducible tool for the esterification of polysaccharides. But these synthesis methods are limited for the preparation of common aliphatic or aromatic carboxylic acids esters. To achieve acylation, a broad variety of new synthesis paths are under investigation.

Once we were able to obtain fluorinated cellulose esters, the nanoprecipitation technique was done in order to create the nanospherical fluorinated cellulose esters. Inspired by natural superhydrophobic surfaces, the micro- and nano-structured surfaces are a crucial factor for constructing artificial superhydrophobic surfaces. Despite, the micro- nanostructured surface can influence on the movement of the water droplet. In fact the hydrophobicity character depends on the surface roughness that is created by micro- and nano-scale hierarchy[3].

3. Superhydrophobicity from cellulosic materials

3.1. Superhydrophobic cellulose nanocrystals

Superhydrophobic surfaces create a contact angle of water that is larger than 150° and water droplet can roll off the surface easily when the surface is tilted up slightly. One of the excellent examples of superhydrophobic surface in nature is the lotus leaf. In fact, this lotus leaf consists of micro- and nano-scale papillae that are coated on a hydrophobic wax. Such a micro- nanostructured surface can influence the movement of the water droplet[32]. This result from the natural superhydrophobic surfaces found out a way for constructing the artificial hydrophobic and superhyrophobic surfaces similar to the surface of the lotus leaves. Superhydrophobic surfaces are particularly interesting due to the great variety of potential application such as self-cleaning, the packaging industry, coating industry, medical device, and microfluidic device. A number of chemical surfaces treatments have been investigated such as the silylation or fluorination of both synthetic polymers and inorganic compounds, respectively[33,34,35].

Generally, both the surface chemistry and the surface roughness affect hydrophobicity and the interplay between these properties have been the subject of active research during the last decades. Techniques to endow the surface with nano-scale roughness, such as etching and lithography, sol-gel processing and electro spinning have been implemented while the surface chemistry has been modified by using strategies involving physical and chemical adsorption. A distinctive feature is the fact that substrates based on non-renewable materials, including minerals and synthetic polymers, are being substituted as platforms to develop superhydrophobic surfaces. However, efforts to induce hydrophobicity in bio-based materials, including cellulose, are growing and are being reported more often. Many developments to obtain superhydrophobic surfaces based on cellulose have been reported in recent years, for example in cotton fabrics and paperboard[36].

As mentioned at introduction part, cellulose is an abundant, inexpensive, biodegradable and renewable biopolymer which contains very good mechanical properties. There are different techniques for modifying cellulose into hydrophobic derivatives like etherification[37], fluorination[38], silyation[39] or grafting by using polymers[40]. Obviously, hydrophobic properties of products depend on the initial material chemical properties. Usually from these methods the modified cellulose derivatives are not so hydrophobic and they still absorb water. Esterification of cellulose with long chain fatty acid esters helps to introduce more hydrophobic properties of modified cellulose[41,42].

Generally, the modification of polysaccharides with hydrophobic functional groups has been carried out with acetyl, propyl and cholesteryl groups[43]. However, we have used long chain fluorinated fatty acids in order to gain more hydrophobic cellulose ester as our final target. Due to the abundance of OH groups in cellulose, chemicals with low surface energy, such as fluorine containing substitutes can be easily introduced by esterification with acids or anhydrides[36]. The modified cellulose esters have been utilized for paper coating in order to introduce superhydrophobic or/and very hydrophobic properties.

Scanning electron microscopy (SEM), transmission electron microscopy (TEM) and atomic force microscopy (AFM) are some of the tools that have enabled the observation of nano-scale features on the surfaces and to unveil some of the secrets behind superhydrophobic development. The combination of low surface energy and nanoroughness are effective in attainment of superhydrophobicity.

The approaches used in recent years toward superhydrophobicity of cellulosic materials can be classified into two categories, based on the generation of roughness: (1) Roughness offered by coating cellulosic substrates, which include: a) Chemical grafting to modify the surface chemistry and surface morphology of cellulosic fiber/surface simultaneously. b) Sol-gel processes to render cellulose fiber/surface with porous outer-layer and to reduce surface energy by post-treatment or by mixing precursors with low surface energy side chains. c) Nanoparticle deposition, for example by using metal, metal oxide, mineral and polymers that modify the morphology of the cellulosic fiber/surface, followed by surface energy reduction by post-treatment. d) Chemical vapor deposition. (2) Roughness offered by regeneration or fragmentation of cellulosic materials, which among others include: e)

Electrospinning and elecrospraying f) Use of nanocellulose (cellulose nanocrystals and nanofibrillated cellulose). g) Use of cellulose composites[36].

The stable suspension of cellulose ester nanoparticles in water was implemented via nanoprecipitation technique. After esterification of cellulose, nanoparticles of cellulose ester were obtained through nanoprecipitation technique in aqueous suspension[44]. Nanoprecipitation technique is a facile, mild, and low energy input process for the preparation of polymeric nanoparticles. This technique is also known as solvent diffusion, solvent shifting, and diafiltration method.

Nanoparticle formation via this technique results from a dilution of the solute molecules in a non-solvent, causing the nucleation of very small aggregates of solute molecules which is followed by aggregation of these nuclei (nucleation-aggregation mechanism). This nanoprecipitation technique starts with aggregation process and stops when colloidal stability is reached[45]. In fact there are two different nanoprecipitation techniques, the dropping and the dialysis methods. In this study the dropping technique was applied. The advantage of the dialysis technique is the complete exchange of the polymer solvent against the non-solvent. However, this method is relatively time-consuming, and may not be suitable for less stable particle system. The dropwise addition of the polymer solution to the non-solvent is usually applied when the system contains a volatile solvent, because it is easy to evaporate and eventually leads to pure nanoparticle suspensions. The type of solvent and non-solvent, the quality of solvent (pH, salt concentration), and the polymer concentration have a crucial effect on the final nanoparticle suspension[46].

In this study, the very hydrophobic and superhydrophobic coating of paper surface was carried out by using solutions of cellulose 2H,2H,3H,3H-perfluorononanoic ester and cellulose 2H,2H,3H,3H-perfluoroundecanoic ester, respectively.

3.2. Paper coating

The coating method can be classified into three different methods such as dip coating, spin coating, and spray coating. We have changed the hydrophilic properties of paper into superhydrophobic properties by spin coating the surface with a suspension of nanofluorinated cellulose esters. The superhydrophobic surface shows a water contact angle larger than 150°. Recently, many techniques have been developed for the fabrication of superhydrophobic paper surface, e.g. via plasma enhanced etching and deposition[47], wax mixture coating[48], by spraying silica nanoparticles onto the paper[49], with multi-layer deposition which follows by a simple electroless galvanic deposition method[50], and also surface coating using multiple dip coating with alkyl ketone dimer[51], spraying with rapid expansion of supercritical CO_2 with alkylketene dimmers (AKD)[52], and ink-jet printing[53]. In addition to these methods, the spin coating of nanostructured fluorinated cellulose esters is a fast and simple method meanwhile after coating there is no need for further modification of the paper surface.

Paper is one of various materials that are used very often in our daily life. Paper has recently attracted significant attention due to several unique inherent properties, such as high flexibility, high strength, biodegradability and renewability[54]. In recent years there is an increasing demand for hydrophobic/superhydrophobic papers, since they can use for a range of area stretching from food packaging to inkjet printing. In fact, having self-cleaning and thermal resistance properties of this superhydrophobic surface leads to the wide range of the various applications. Generally, studies on superhydrophobic paper are limited since the methods are too tedious. However, simple coating of paper surface by nanostructured fluorinated cellulose esters leaded to superhydrophobic paper surfaces.

4. Results and discussion

In this chapter, the results achieved in this study will be discussed in detail: first, the esterification of CNCs, which was needed to acquire superhydrophobic cellulose ester modified fluorinated cellulose ester. Then, our study focuses on the synthetic methods used and on the investigations regarding the properties of those obtained nanospherical fluorinated cellulose esters that were coated on the paper's surface.

4.1. Synthesis of 2H,2H,3H,3H-perfluorononanoyl chloride and cellulose 2H,2H,3H,3H-perfluorononanyl ester

As noted, cellulose esterification with acid chloride in the presence of pyridine results in high yields of products. Therefore, the synthesis of the 2H,2H,3H,3H-perfluorononanoyl chloride from the 2H,2H,3H,3H-perfluorononanic acid with thionyl chloride as a solvent was necessary to synthesize the cellulose 2H,2H,3H,3H-perfluorononanyl ester. Figures 12 and 13 present the conversion of the 2H,2H,3H,3H-perfluorononanic acid into the 2H,2H,3H,3H-perfluorononanoyl chloride. According to Figure 13, two triplet ^{1}H NMR peaks at ~ 3.26 and 2.85 ppm show the presence of hydrogen atoms that are adjacent to the carbonyl of acyl chloride. More details regarding the synthesis can be found in the experimental part of this paper on page 36.

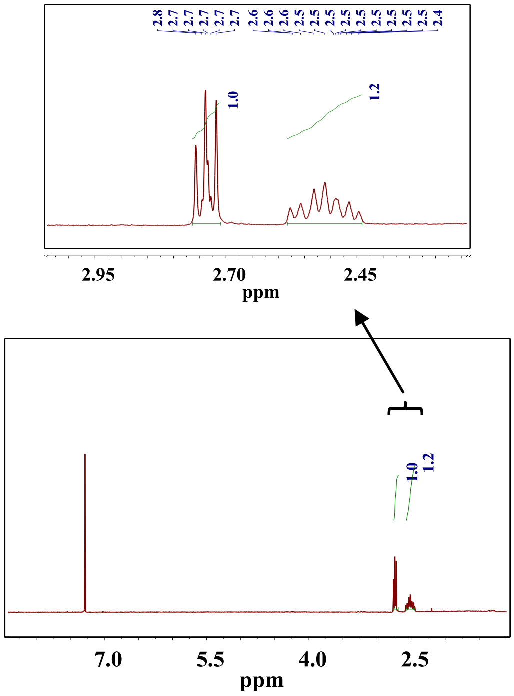

Figure 12. [1]H NMR spectra of the 2H,2H,3H,3H-perfluorononanoic acid in $CDCl_3$.

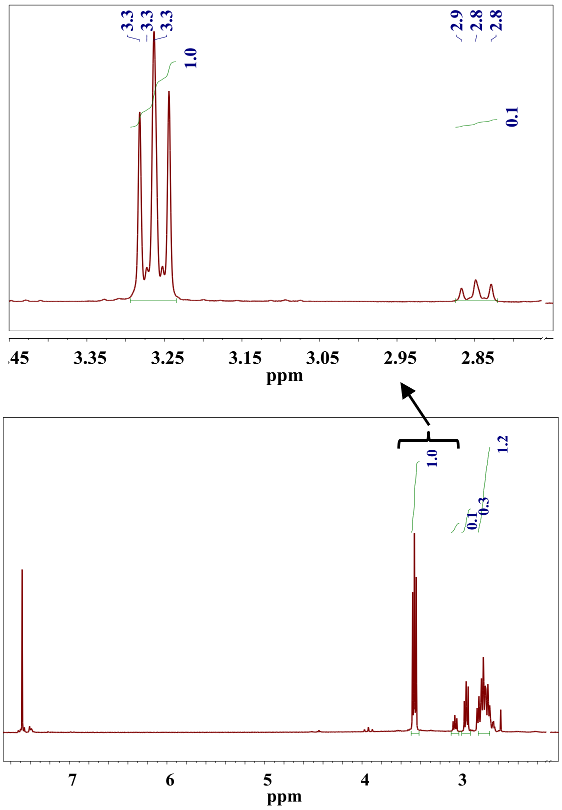

Figure 13. [1]H NMR spectra of the 2H,2H,3H,3H-perfluorononanoyl chloride in $CDCl_3$.

Once the 2H,2H,3H,3H-perfluorononanoyl chloride was successfully synthesized, the esterification reaction of CNCs with this 2H,2H,3H,3H-perfluorononanoyl chloride was carried out in the presence of pyridine and toluene (The details of the synthesis are explained in the experimental section of this chapter). Therefore, cellulose 2H,2H,3H,3H-perfluorononanyl esters are compounds consisting of cellulose chains and 2H,2H,3H,3H-perfluorononanyl groups.

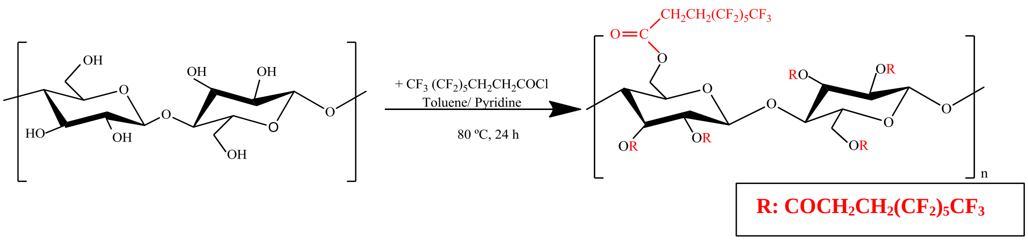

Figure 14. Schematic representation of the synthesis of cellulose 2H,2H,3H,3H-perfluorononanyl ester.

After synthesizing the cellulose esters, they were characterized by FT-IR and solid state NMR spectroscopy. Based on this analysis, the presence of both ester-functional groups is obviously recognizable. The signal at 1753 and 1750 cm^{-1} in Figure 15, is related to the C═O stretching vibrations of ester bonds, respectively.

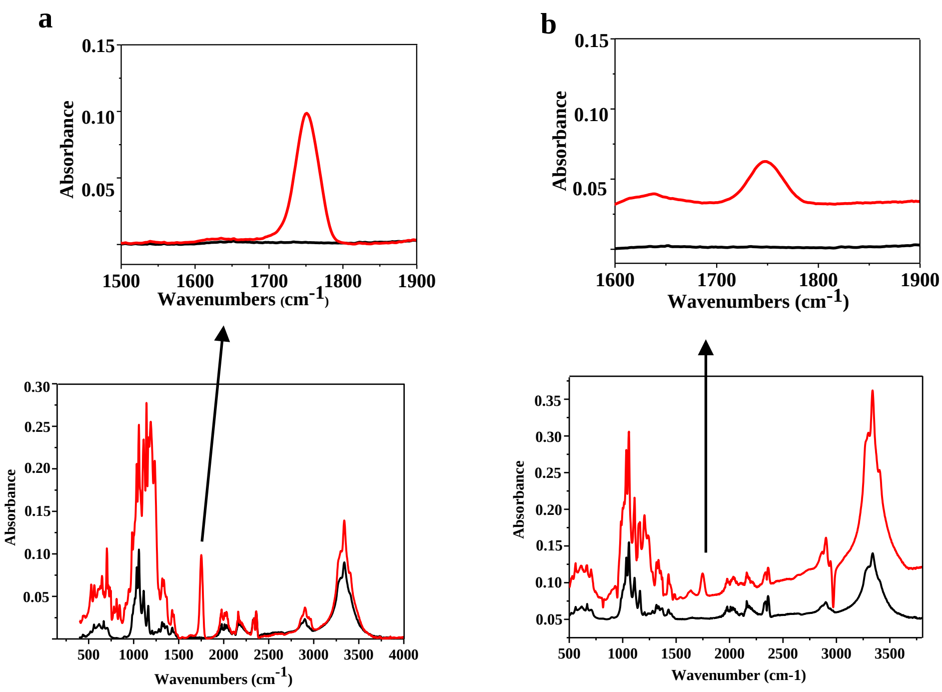

Figure 15. a) FT-IR spectrum (4000-500 cm^{-1}) of cellulose nanocrystal (black) and cellulose 2H,2H,3H,3H-perfluorononanyl ester (red). b) FT-IR spectrum (4000-500 cm^{-1}) of cellulose (black) and cellulose 2H,2H,3H,3H-perfluoroundecanoyl ester (red).

IR ν_{max} cm^{-1} 735.40m (C-C rocking vibration), 1142.54s (C-O-C), 1427.54 (CH_2CO), 1233.43s (CF_2), 1317.73s, 702.57m (CF_3), 1750.86s (C=O), 3339.85m (OH).

4.2. Synthesis of cellulose 2H,2H,3H,3H-perfluoroundecanoyl ester

The synthesis of modified cellulose esters was attempted by esterification of CNCs by means of 2H,2H,3H,3H-perfluoroundecanoyl chloride. CNCs have a high aspect ratio (3–5 nm wide and 50–500 nm in length), and as a result, they exhibit more reactivity. As expected, the degree of substitution with sulfate groups increases with increasing hydrolysis time. These sulfate groups are charged and it leads to create a more stable suspension in various organic solvents such as pyridine and toluene. The three hydroxyl groups in each glucose unit of the cellulose chain are able to react with inorganic and organic acids or their anhydrides and chlorides to form esters. During the reaction with inorganic acids the polar OH-groups are substituted by nucleophilic groups in a strong acid environment. All reaction steps are reversible and equilibrium conditions have been attained. However, esterification can be promoted with water-binding catalysts, such as concentrated sulfuric acid, phosphorous acid, phosphorus or acetic anhydride. The focus of our study was to prepare cellulose esters by the addition of acid chlorides in the presence of a base, rather than acid catalysts. Since the level of the base diminished during the reaction, the esterification is most likely a base-catalyzed process.

The CNC substrates were esterified with 2H,2H,3H,3H-perfluoroundecanoyl chloride in the presence of pyridine and toluene. The molar ratio of 2H,2H,3H,3H-perfluorononanoyl chloride per anhydroglucose unit of cellulose was 1.5. As Figure 16 shows, the cellulose 2H,2H,3H,3H-perfluoroundecanoyl ester compound consist of cellulose chains and 2H,2H,3H,3H-perfluoroundecanoyl groups.

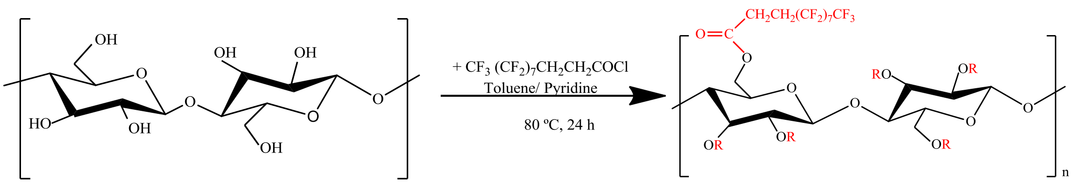

Figure 16. Scheme of Scheme of the synthesis of a 2H,2H,3H,3H-perfluoroundecanoyl cellulose ester.

IR spectroscopy of cellulose 2H,2H,3H,3H-perfluoroundecanoyl ester shows the characteristic signal at 1753 cm^{-1}, which is characteristic for the carbonyl of an ester group (C=O stretch).

IR ν_{max} cm^{-1} 657.62 (C-C rocking vibrations), 1146.19s (C-O-C), 1200.13s (CF_2), 703.91s-1334.39s (CF_3), 1428.84 (CH_2CO) 1753.36 (C=O), 3339.06m (OH).

The esterification of CNCs was attempted with two different acid chlorides: 2H,2H,3H,3H-perfluorononanoyl chloride and the 2H,2H,3H,3H-perfluoronodecanoyl chloride. Their only difference is the chain length and thus the number of fluoro functional groups. However, based on the characterization techniques applied, no significant difference in the hydrophobic properties of the resulting cellulose esters was detected. In fact, the higher DS value, influenced to achieve more hydrophobic cellulose ester and breaking the hydrogen bonding network, which leads to enhance the solubility of modified cellulose esters into different non-polar solvents. Moreover, tuning the perfluorinated acyl chloride concentration and amount of the pyridine has a significant effect on the DS value.
Cellulose esters were also characterized by solid-state ^{13}C NMR spectroscopy (Figure 17). The set of spectra includes resonance peaks in the range of 55 to 110 ppm, corresponding to the cellulose carbon atoms. The cellulose ester samples reveal additional resonances, one near 173 ppm, characteristic for the ester group, and others in the range 20 to 35 ppm, characteristic for the carbons from the aliphatic chains of the 2H,2H,3H,3H-perfluoroundecanoyl chloride and the 2H,2H,3H,3H-perfluorononanoyl chloride. Figure 17 shows a pronounced peak at 92 ppm, part of the C-4 resonance and characteristic for the crystalline structure of cellulose, while the broader peak of C4, near 85 ppm was attributed to the amorphous part of the cellulose 2H,2H,3H,3H-perfluorononanyl ester.

The resonance of the carbonyl group of cellulose 2H,2H,3H,3H-perfluorononanyl ester is sharper than cellulose 2H,2H,3H,3H-perfluoroundecanoyl ester. Therefore it may be assumed that the cellulose 2H,2H,3H,3H-perfluorononanyl ester has a higher DS than the 2H,2H,3H,3H-perfluoroundecanoyl ester. ^{13}C NMR (8 kHz) δ 27.33 ($CH_2CH_2(CF_2)_5CF_3$); δ 67.58 (C_{cell}-6); δ 73.65-76.93 (C_{cell}-2,3,5, C_{ester}-2,3,5); δ

90.87 (C_{cell}-4); δ 106.42-108.02 (C_{cell}-1, C_{ester}-1); δ 173.28 (C=O). The higher solubility in tetrahydrofuran (THF) also indicates a higher DS value of the former.

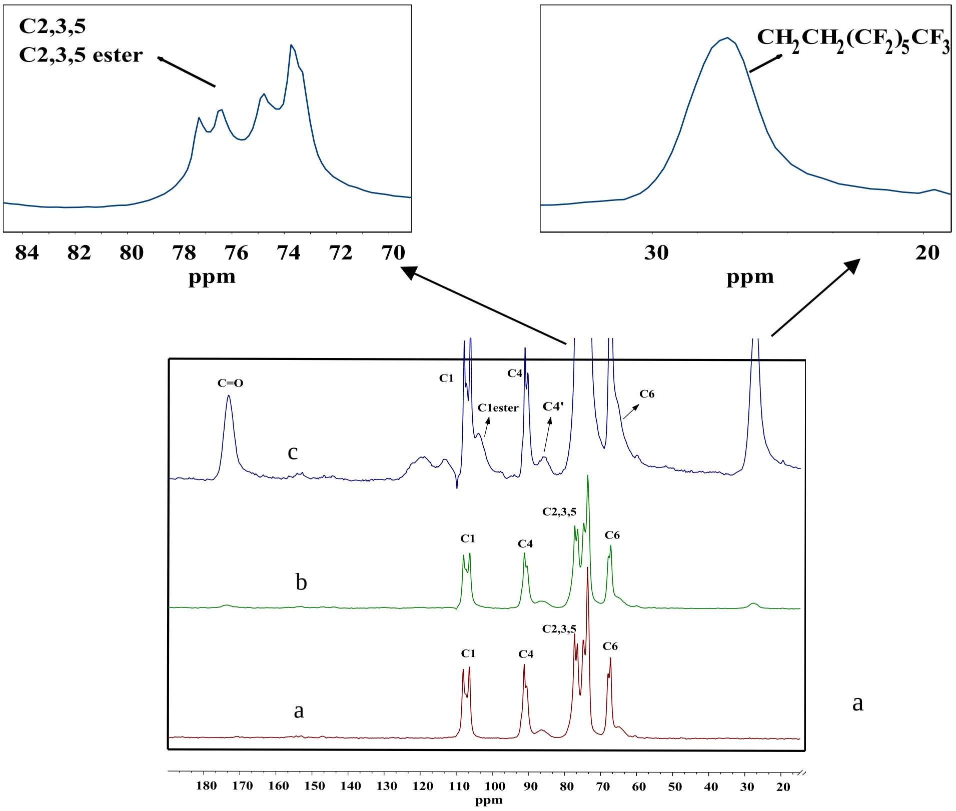

Figure 17. Solid-state ^{13}C NMR spectra of CNCs (a), cellulose 2H,2H,3H,3H-perfluoroundecanoyl ester (b), and cellulose 2H,2H,3H,3H-perfluorononanyl ester (c).

In order to determine how the crystalline structure in CNCs was changed during the esterification and nanoprecipitation, XRD measurements were utilized. Figures 18 and 19 depict the X-ray diffraction patterns of CNCs, cellulose esters, and nanostructured cellulose esters. The reduced intensity of the peak at the 002 plane demonstrates the reduction of crystalline-ordered scattering units resulting from a significant destruction of the crystalline structure. There is also an increased intensity in the amorphous region of cellulose esters at around 18º, which is attributed to the less ordered region of cellulose chains[55]. The X-ray diffraction peaks of nanostructure cellulose esters acquire broader at lower angles. These peaks may come from a smaller size of cellulose crystallites. However, it has to be considered that an amorphous region of disordered cellulose esters or an amorphous ester can appear at angles around 18º–20º[56]. Nevertheless, cellulose 2H,2H,3H,3H-perfluorononanyl ester clearly indicates an amorphous structure by the absence and strong reduction of all peaks corresponding to planes (101), (10^{-}1), and 002. However, there is more evidence that C4 peaks of solid-state ^{13}C NMR are related to the interior crystalline cellulose structure but the C4´ peak relates to the amorphous structure.

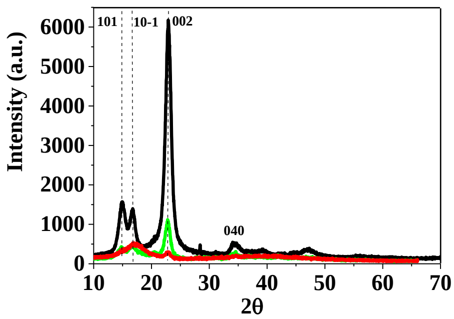

Figure 18. XRD of CNCs (black peak), cellulose 2H,2H,3H,3H perfluorononanyl ester (red peak) and cellulose 2H,2H,3H,3H-perfluoroundecanoyl ester (green peak).

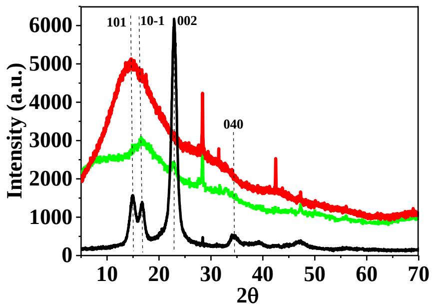

Figure 19. XRD of CNCs (black peak), NPs of cellulose 2H,2H,3H,3H-perfluorononanyl ester (red peak) and cellulose 2H,2H,3H,3H-perfluoroundecanoyl ester (green peak) after nanoprecipitation dropping technique.

The sharp peak that is located at 28º in Figure 19 is related to the Si substrate[57]. The crystalline size value was calculated using the well-known Scherrer formula[58] :

$$D = \frac{k\lambda}{\beta\cos\theta}$$

Where, k is the Scherrer constant (0.9), λ is the wavelength of the X-ray (λ=0.154 nm), β is FWHM (full width at half maximum) of the (002) peak, and θ is the diffraction angle of the (002) plane. The dimension of crystallites from the X-ray data obtained from the fitted spectra is shown in Figure 20.

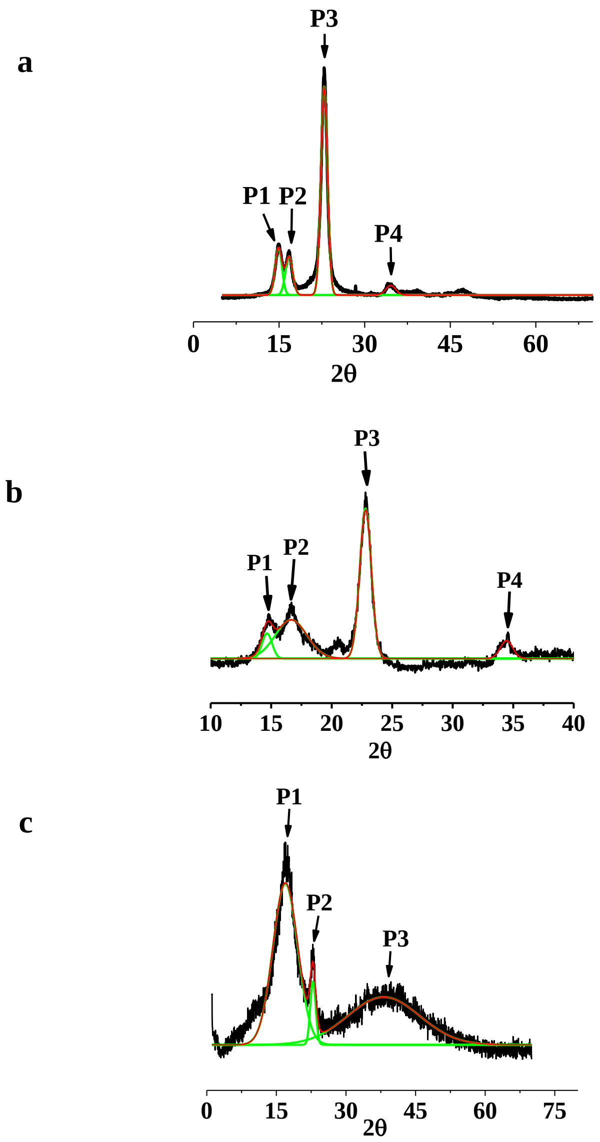

Figure 20. Resolution of X-ray diffraction curves of CNCs (a), cellulose 2H,2H,3H,3H-perfluorononanyl ester (b) and cellulose 2H,2H,3H,3H-perfluoroundecanoyl ester (c).

According to Figure 20, the diffraction pattern of cellulose esters is similar compared with the diffraction patterns measured from CNCs. These results come from changing the crystallite dimension (Table 3). The four peaks in the XRD spectra (P1, P2, P3, and P4) represent the latice planes of (1¯10), (110), (200), and (004), respectively. The 2θ value of all the diffraction peaks are listed in Table 4.

Table 3. 2θ values of reflections of XRD patterns.

Reflection	**2θ value (º)**		
	CNC	**Cellulose Perfluoroundecanoyl ester**	**Cellulose Perfluorononanyl ester**
P1	14.90	14.66	16.99
P2	16.75	16.64	22.84
P3	22.90	22.79	38.17
P4	34.55	34.44	-

Table 4. Crystalline size calculated from XRD patterns.

Samples	**d_{002} (nm)**
CNC	5.84
Cellulose Perfluoroundecanoyl ester	7.18
Cellulose Perfluorononanyl ester	5.6

It is well known that the crystallinity of cellulose can be measured by means of solid-state ^{13}C NMR, XRD, etc. Solid state ^{13}C NMR considers contributions from both crystalline and non-crystalline cellulose regions, resulting in relative values, while the XRD approach gives more detailed data on crystalline and non-crystalline the fractions of cellulose. It was shown that the crystal structure of CNC's was altered by both esterification and nanoprecipitation treatments. Two different nanoparticle preparations methods: dropping and dialysis techniques can be applied to manufacture the nanoparticles, as is shown in Figure 21[59]. In this study nanoprecipitation was a suitable technique to construct a stable nanospherical fluorinated cellulose ester suspension.

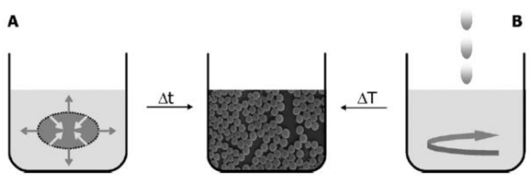

Figure 21. Nanoprecipitation methods applying dialysis in a membrane (A) and dropping technique (B), respectively[59].

Since the total amount of the cellulose esters is distributed homogenously throughout the solution during nanoprecipitation, the particles are inclined to form a spherical shape. Nanoprecipitation is interesting for preparing colloids for stabilizing pigments[60], and for industrially important components in paints, lacquers, and other coatings[46].

Strong hydrogen bonding network and the hydrophobic interaction of CNCs prevent dissolution into the most common organic solvents. However, the solubility of CNCs can be improved by surface functionalization. For example, the solubility of perfluorinated cellulose esters in THF was increased by progressive derivatization. In fact, the substitution of the hydroxyl groups, e.g. by acyl chlorides, leads to the breakage of the hydrogen bond network of cellulose and therefore enhances the solubility in organic solvents. Increasing solubility of cellulose esters and providing a stable suspension of nanostructured cellulose esters, are crucial factors in order to obtain more uniform coatings on different surfaces.

The solubility of cellulose esters was tested in different non-polar solvents. Actually, the solubility depends on the DS and the chain length of the acyl chlorides[61]. Both fluorinated cellulose esters are mostly insoluble in non-polar solvents (such as hexane, pentane, benzene, and toluene). However, in this study, THF created a more transparent suspension of perfluorinated cellulose esters with less aggregation compared to the other solvents. Cellulose esters formed a stable suspension in THF, which could be successfully used as the initial formulation for the nanoprecipitation into deionized water.

The nanostructured fluorinated cellulose esters were analyzed for size and shape by scanning electron microscopy (SEM) and dynamic light scattering (DLS). Figure 22 shows nanospheres of 2H,2H,3H,3H-perfluorononanyl ester and 2H,2H,3H,3H-perfluoroundecanoyl ester at different concentrations, respectively.

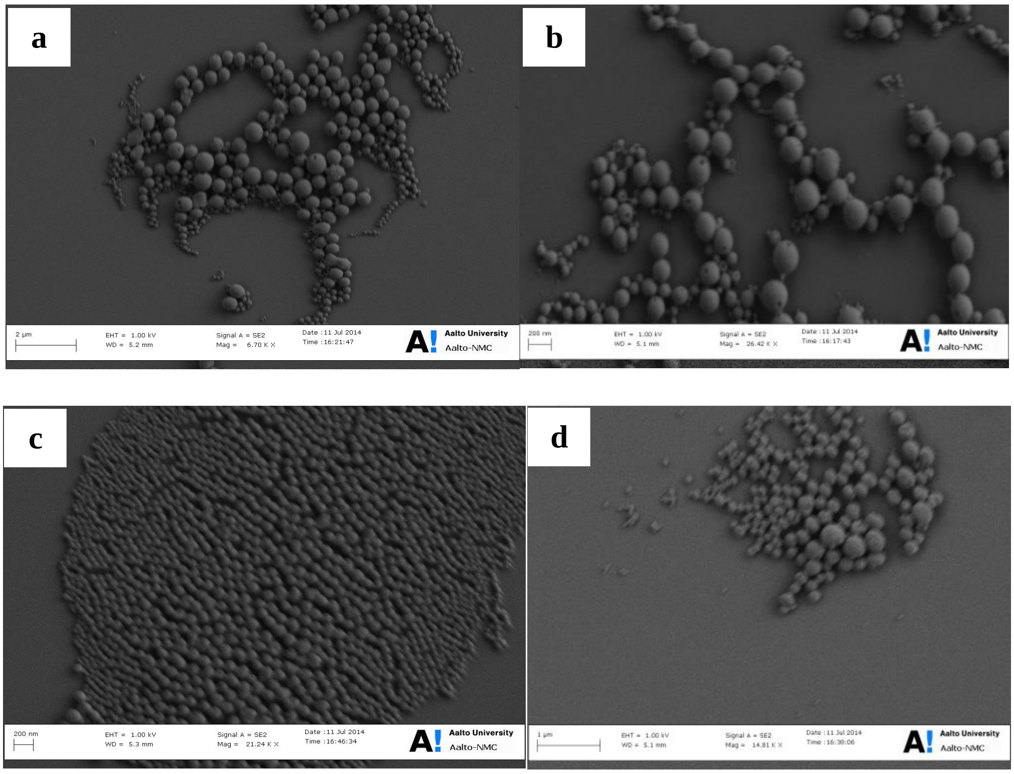

Figure 22. SEM images of NPs from 2H,2H,3H,3H-perfluorononanyl ester (a, b) and 2H,2H,3H,3H perfluoroundecanoyl ester (c, d) from various concentrations: 1 mg/ml (a and b), 0.1 mg/ml (c) and 10 mg/ml (d).

Since cellulose esters suspended in THF do not interact with water, the formation of nanoparticles is based on the aggregation of cellulose ester chains during the diffusion of drops of cellulose suspension into deionized water. During this fast process, there is a large contact area between the drops of cellulose ester suspension and water which promotes the mixing of THF and therefore the aggregation of cellulose ester chains[44]. After the removing of THF, cellulose esters start shrinking, and eventually, nanostructured fluorinated cellulose esters can be formed.

Nanostructured 2H,2H,3H,3H-perfluoroundecanoyl ester resulting from the nanoprecipitation dropping technique had an average diameter of 180±0.4 nm with a polydispersity index of 0.309 (Figure 23). The DLS measurements were repeated three times; that result from each measurement are presented in Table 5.

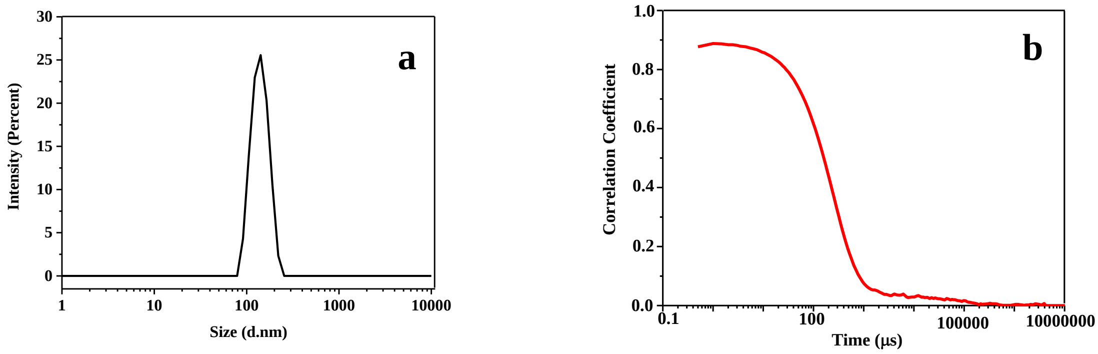

Figur 23. Size distribution of cellulose ester nanoparticles (a) and autocorrelation curve of DLS measurements (b).

Table 5. measurements of 2H,2H,3H,3H-perfluoroundecanoyl ester nanoparticles.

Run	Z-Average (*d*, in nm)	Polydispersity index
1	186.1	0.317
2	184.0	0.326
3	180.4	0.309

The difference between average diameters obtained from SEM and DLS is related to different techniques at each measurement. In the DLS measurement, the fluorinated cellulose ester nanoparticles may be slightly swollen in deionized water. That it shows larger hydrodynamic diameter. On the contrary, samples were dried for SEM measurement.

In this study different surfaces such as glass, and different types of hydrophilic and hydrophobic papers were coated. We were successful in fabricating a superhydrophobic surface only on a normal hydrophilic paper surface. According to Figure 24, the contact angles of coated paper are higher than 160°, while the surface contact angle measurement of uncoated paper was impossible since the water droplets quickly penetrate the paper after only a few minutes. We also tried to obtain a more homogeneous coating by utilizing a more dilute nanoparticle suspension.

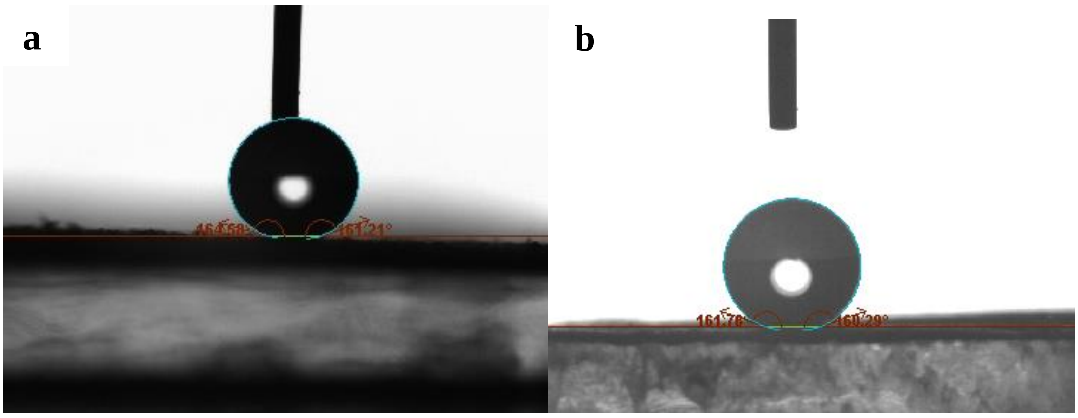

Figure 24. Photos of static contact angle measurement on paper surface which were coated by 2H,2H,3H,3H-perfluorononanyl ester (a) and 2H,2H,3H,3H-perfluoroundecanoyl ester (b).

Geissler et al. constructed nanostructured stearoyl cellulose ester[44], which was used for coating paper[62] and glass surfaces[63]. They have shown that that the initial concentration of cellulose ester suspension at nanoprecipitation techniques has a significant effect on the size of the obtained nanoparticle[44]. However, in our work, we only could obtain a superhydrophobic surface on a paper surface where the static CA is larger than 160º. Both perfluorinated acyl chlorides that have been utilized create very hydrophobic cellulose esters. As Table 6 shows, the water contact angle critically depends on the initial concentration of cellulose esters. In this study, the contact angles of water droplets on the paper surface are comparable to the paper surfaces coated with cellulose stearoyl ester.

Table 6. Water contact angles of superhydrophobic paper stripes that have been dip-coated with CSE solution with different concentrations and spray-coated using cellulose stearoyl ester (CSE)[62].

Dip-coated using CSE solution of	**Water contact angles (º) after**		
	15s	**30s**	**180s**
1 1 mg/ml	147.9	146.6	143.6
2 5 mg/ml	151	152.4	151.6
3 10 mg/ml	151.2	154.4	152.6

The minimum concentration of fluorinated cellulose ester suspension that created a paper's superhydrophobic surface was 5 mg/ml. Here the water droplet contact angle was around 160º. As was mentioned previously, the solubility of modified cellulose esters in organic solvents such as THF was increased with increasing degree of substitution. It has to be considered that, in the current study, we obtained a very hydrophobic paper surface while the molar ratios of 2H,2H,3H,3H-perfluoroundecanoyl chloride and 2H,2H,3H,3H-perfluorononanoyl chloride to an anhydroglucose unit of cellulose were only 1.5 and 3, respectively. However, Geissler et al. have used higher ratio of stearoyl acid chloride in order to obtain a superhydrophobic glass and paper surface (The molar ratios of stearoyl acid chloride per mol of anhydroglucose units of cellulose is 6)[62]. Obviously, the superhydrophobicity can be improved at a higher DS of cellulose esters. The DS of cellulose esters is greatly influenced by the ratio of acyl chloride-to-cellulose hydroxyl groups, the reaction temperature, the reaction time, and also the volume ratios of pyridine/toluene that are utilized.

5. Conclusion

In recent years, there is an increasing demand for special papers including hydrophobic/superhydrophobic papers, since they have various applications like food packaging, paper based sensors, and protection of valuable old documents, etc. Research on superhydrophobic surface especially on paper is fairly a new area, and only very limited scientific publications are available in the literature. Superhydrophobicity has been achieved on paper surface via different techniques such as plasma enhanced etching, chemical vapor deposition of composites of silica and polymers, etc. Among these available techniques, cellulose functionalization like esterification method is very facile, time saving and they can be carried out without special equipment.

The main findings of this work can be divided into two parts. First, we achieved the superhydrophobic fluorinated cellulose esters by the esterification of CNCs. Secondly, spin coating was applied to translate superhydrophobic properties of the modified cellulose to the surfaces of several substrates. The modification efficiency was proved by spectrometric analysis and the examination of dispersion properties. We demonstrated that the fluorinated cellulose ester with a higher DS, indicated by ^{13}C NMR and IR spectroscopy, provides a more transparent suspension in THF. In fact, the solubility of fluorinated cellulose esters was enhanced in comparison with unmodified CNCs. However, XRD and ^{13}C NMR analyses showed that the morphology and structure can be changed by both esterification and nanoprecipitation techniques. Both the long and perfluorated alkyl chains had a significant effect on gaining thermal resistance and very hydrophobic nanostructured cellulose esters. Paper with super-hydrophobic surface properties may be used in packaging materials, textiles, outdoor clothing, and microfluidic devices. In the future, it would be highly interesting to find a way, such as optimization of DS, to achieve a more stable and uniform superhydrophobic surface on various substrates such as glass, textiles, etc.

6. Experimental

This chapter gives a short description of material and methods used in this thesis. All reagents of cellulose nanocrystals (CNCs), 4,4,5,5,6,6,7,7,8,8,9,9,9-tridecafluorononanoic acid, thionyl chloride, and 4,4,5,5,6,6,7,7,8,8,9,9,10,10,11,11,11-heptadecafluoroundecanoyl chloride, were utilized as received (Sigma-Aldrich) without further purification. The used CNCs, were extracted from one of the most popular, accessible, and reproducible cotton filter paper.

6.1. Synthesis of 2H,2H,3H,3H-perfluorononanoyl chloride

Excess freshly $SOCl_2$ (7 ml) was added to 2H,2H,3H,3H-perfluorononanoic acid (3 g, 7.65 mmol) and it was stirred under an atmosphere of N_2 for 12h to yield 2H,2H,3H,3H-perfluorononanoyl chloride (2.60g, yield 87%) as yellow oil. The excess thionyl chloride removed under vacuum and dried toluene was added to the oil. This was stirred for 15 min and then the solvent was removed by vacuum to produce yellow oil.

$$CF_3(CF_2)_5CH_2CH_2\mathbf{COOH} \xrightarrow{\mathit{SOCl_2}} CF_3(CF_2)_5CH_2CH_2\mathbf{COCl}$$

All spectra recorded on a Bruker (^1H 400 MHz, ^{13}C 100 MHz) spectrometer. According to Figure 13, two triplet peaks at ~ 3.5 and 2.85 ppm show the presence of hydrogen atoms that are adjacent to the carbonyl of acyl chloride. ^1H NMR ($CDCl_3$, 400 mHz) δ 2.56 (t, $C\mathbf{H_2}CF_2$, 2H); δ 2.85 (t, $^3J_{HH}$ = 8 Hz, $C\mathbf{H_2}CH_2COCl$); δ 3.26 (t, $^3J_{HH}$ = 8 Hz, $C\mathbf{H_2}COCl$, 2H).

6.2. Synthesis of cellulose 2H,2H,3H,3H-perfluorononanyl ester

200 mg freeze-dried CNCs were dispersed in 10 ml pyridine. Then, the cellulose suspension was heated up to 80 °C and 1.5 g 2H,2H,3H,3H-perfluorononanoyl chloride (3.65 mmol) was dissolved in 10 ml toluene and was dropped into the hot cellulose suspension, while it was under nitrogen atmosphere. After 24 h stirring at 80 °C, the reaction mixture was poured into 100 ml toluene. The precipitate was

purified by centrifugation, purified through repeated dispersion in dichloromethane and precipitate in ethanol. The dried products under vacuum were characterized by FT-IR (Figure 14) and solid state ^{13}C NMR spectroscopy (Figure17). Fourier transform-infrared (FT-IR) spectra were recorded on a Nicolet Magna 750 instrument. **IR** ν_{max} cm^{-1} 735.40m (C-C rocking vibration), 1142.54s (C-O-C), 1427.54 (CH_2CO), 1233.43s (CF_2), 1317.73s, 702.57m (CF_3), 1750.86s (C=O), 3339.85m (OH).

6.3. Synthesis of cellulose 2H,2H,3H,3H-perfluoroundecanoyl ester

80 mg freeze-dried CNCs were dispersed into 10 ml pyridine. Then, the cellulose suspension was heated up to 80 °C and 1 g 2H,2H,3H,3H-perfluoroundecanoyl chloride (1.96 mmol) was dissolved in 10 ml toluene and were dropped into the hot cellulose suspension, while it was under nitrogen atmosphere. After 24 h stirring at 80 °C, the reaction mixture was poured into 100 ml toluene. The precipitate was purified by centrifugation, purified through repeated dispersion in dichloromethane and precipitate in ethanol. Finally, product was dried under vacuum. **IR** ν_{max} cm^{-1} 657.62 (C-C rocking vibrations), 1146.19s (C-O-C), 1200.13s (CF_2), 703.91s-1334.39s (CF_3), 1428.84 (CH_2CO) 1753.36 (C=O), 3339.06m (OH). ^{13}C NMR (8 KHz) δ 27,33 ($CH_2CH_2(CF_2)_5CF_3$); δ 67.58 (C_{cell}-6); δ 73.65-76.93 (C_{cell}-2,3,5, C_{ester}-2,3,5); δ 90.87 (C_{cell}-4); δ 106.42-108.02 (C_{cell}-1, C_{ester}-1); δ 173.28 (C=O).

6.4. Nanoprecipitation of modified cellulose

Nanoparticles of the modified cellulose were prepared via the dropping nanoprecipitation technique. Before the nanoprecipitation, modified cellulose was dissolved in THF at different concentrations: 0.1 mg/ml, 1 mg/ml and 10 mg/ml. The solution was filtered through a filter paper with the pore size of 1 µm in a Buchner funnel under vacuum[44]. After filtration, 10 ml of solution was precipitated drop by drop into 250 ml deionized water at room temperature (RT). Then, the white suspension was stirred for a 30 min. After that the suspension was heated up to 75 °C for 30 min in order to remove THF. According to Figure 25 after removing THF, cellulose esters start shrinking and forming nanospherical structure.

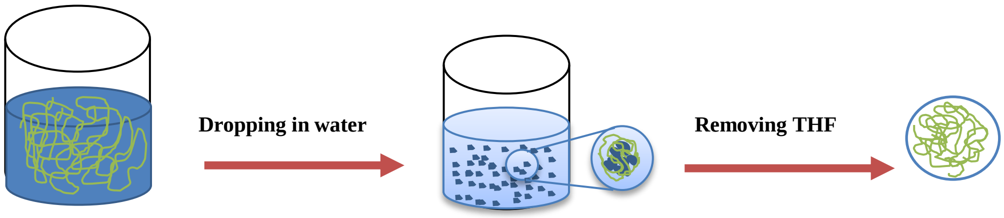

Figure 25. Nanoprecipitation of cellulose ester solution. Green curve: cellulose ester chains and blue dots: THF molecules.

Scanning Electron Microscopy. Studies were performed with a Zeiss Sigma VP Field Emission Scanning Electron Microscope (FE-SEM) operated at 1 kV.

The procedure of sample preparation for SEM measurement: 1 mg/mL of cellulose 2H,2H,3H,3H-perfluorononanyl ester at THF was prepared and the 10 mL of suspension was precipitated drop by drop into the 250 mL of deionized water. Whereas, the initial concentration of cellulose 2H,2H,3H,3H-perfluorononanyl ester at THF was 0.1 mg/mL and 10 mL of suspension was precipitated drop by drop into 250 mL deionized water. The 600 µL of each samples into deionized water were separately dropped into mica substrate. After drying the samples, they were coated with a thin AU layer for 40 seconds.

X-ray diffraction. XRD analysis of the samples was carried out using PANalytical X'Pert Pro MPD Alpha-1, Cu K-alfa1 radiation. The spectra collected in a 2θ range of 2–70º. According to Figures 18 and 19 cellulose 2H,2H,3H,3H-perfluorononanyl ester mostly lost their crystal structure (red peak), but cellulose 2H,2H,3H,3H-perfluoroundecanoyl ester maintain crystal structure (green peak).

Dynamic Light scattering. Nanostructured fluorinated cellulose esters in deionized water measured on Nanosizer (Malvern Instrument Ltd., U.K.) after filter with pore size of 1 µm. 1 mL filtered solution was used for the measurement.

6.5. Preparation of superhydrophobic films

Superhydrophobic surfaces were prepared via dissolving modified cellulose in THF at concentration of 5 mg/mL (Figure 24a) and 25 mg/mL (Figure 24b) and then precipitated into 5 ml and 0.2 ml ethanol, respectively at room temperature. Then spin-coating on the paper surface was carried out. After coating, the paper surface was dried at 50 °C and spin coating was repeated.

Dynamics of coupled chemical systems

Abstract

The dynamics of oscillation in chemical reactions as a research field has grown dramatically over the past 50 years and produced thousands of studies on about 70 known chemical oscillators. Oscillating chemical reactions find many applications in physics, biology, physiology, geology, and medicine[64]. The dynamics of the bromate-sulfite-ferrocyanide (BSF) reaction is studied in a well-mixed open chemical reactor, called a continuous stirred tank reactor (CSTR). A CSTR system can be used to investigate the dynamics of out-of-equilibrium chemical processes, such as oscillation, bistability, and chaos[65]. This BSF reaction exhibits periodic oscillation as a function of $[H^+]$, called pH oscillation. The reaction was carried out at 25ºC, and the flow rate was 1 and 2 mL/min. The pH oscillation occurs only in a specific range of flow rates. Here, we show regular pH oscillation in a BSF system by utilizing different concentrations under a nitrogen atmosphere. Such a pH oscillator system can be coupled or probed with pH-sensitive systems, and it helps to understand new mechanisms may arise by periodic behavior[66].

1. Introduction

A chemical oscillation is a complex mixture of reacting chemical compounds, of which the properties of one or more compounds vary periodically in time. Essentially chemical oscillations have been present as long as life itself. Every living system contains chemical oscillators such as heartbeat and brain waves[26] exhibit rhythmical oscillation. There is a large number of oscillating reactions such as Bray-Liebhafsky (H_2O_2-IO_3^- system), Briggs-Rauscher, CIMA (chlorite-iodide-malonic acid) and the Belousov-Zhabotinskii (BZ)[64]. In this project an artificial oscillation system that we have chosen is bromate-sulfite-ferrocyanide (BSF) system which contains pH oscillation[67].

The chemical oscillation reactions never pass through its equilibrium point. Instead, it is a far from equilibrium phenomenon. The best way to study the non-linear chemical dynamics phenomena is working in an open system (can change matter or/and energy with its surroundings). The open system is far from equilibrium and they could exhibit spontaneous self-organization by dissipating energy with surroundings to compensate for the entropy decreases in the system. A closed system must reach equilibrium and so can exhibit only transitory oscillation[68].

The open system can be created by a reactor which allows us to pump fresh reactants continuously into the system and to pump out reached solution so as to maintain a constant volume. Such a device is known as a continuous-flow stirred tank reactor (CSTR). The CSTR has played a crucial role in nonlinear chemical dynamics. By running reaction in the open system like a CSTR, it is possible to have one or more steady states, as well as, time-dependent asymptotic states. In this part describes the materials and methods used under the CSTR.

1.1. Flow reactor and pumps

In the open system that created with CSTR, there is a flow in a solution at a constant flow rate F (mLs^{-1}) and with volume V (mL). By defining the reciprocal residence time $K_{0,}$ the flow can become independent on the reactor geometry[65]:

$$K_0 = F/V \qquad (1)$$

K_0 can be seen as the average time that a molecule spends in the reactor. Note that the fast flow rate through a large reactor is equivalent to a slow flow rate through a small reactor. The volume is constant by removing solution continuously.

As mentioned previously, the CSTR keeps the system far from equilibrium by pumping fresh reactant into the reactor and reactant material out of the system to maintain constant volume. Therefore, two pumps in the CSTR are needed.

The features of CSTR are characterized by several parameters. One of them is the concentration of the input species that fed into the reactant. Another important parameter is rate, which is determined by the stirring rate and the geometry of the reactor[68]. The flow rate or equivalently, residence time are the parameters to realize how the CSTR behaves.

$$\langle\tau\rangle = \frac{1}{K0} = \frac{\text{Volume (mL)}}{\text{Flow rate (mL s}-1)} \qquad (2)$$

Equation 2 shows the average time that the solutions spend in the reactant. The flow rate can be changed through the pump setup (Figure 25).

1.2. pH oscillation in Bromate-Sulfite-Ferrocyanide system

Essentially, designing a pH oscillator is based on having two main composite pathways, the positive feedback pathway that produces H^+, and a negative feedback pathway that removes H^+ from the system. There are different systems that have pH oscillation but we have chosen the BSF system (Edblom et al., 1989)[68].

Table 7. Mechanism of Bromate-Sulfite-Ferrocyanide reaction[68].

Number	Reaction
B1	$BrO_3^- + HSO_3^- \rightarrow HBrO_2 + SO_4^{2-}$
B2	$HBrO_2 + Br^- + H^+ \rightarrow 2HOBr$
B3	$HOBr + Br^- + H^+ \rightarrow Br_2 + H_2O$
B4	$Br_2 + H_2O \rightarrow HOBr + Br^- + H^+$
B5	$2HBrO_2 \rightarrow BrO_3^- + HOBr + H^+$
B6	$Br_2 + HSO_3^- + H_2O \rightarrow 2Br^- + SO_4^{2-} + 3H^+$
B7	$H^+ + SO_3^{2-} \rightarrow HSO_3^-$
B8	$HSO_3^- \rightarrow H^+ + SO_3^{2-}$
B9	$BrO_3^- + 2Fe(CN)_6^{4-} + 3H^+ \rightarrow HBrO_2 + 2Fe(CN)_6^{3-} + H_2O$

The Table 7 shows mechanism of the BSF system. A key element of the mechanism is protonation and deprotonation equilibrium of sulfite-bisulfite.

In B7and B8 (reverse reaction) reactions, sulfite and bisulfite have the following general model:

$$X + H \rightarrow HX \qquad \text{(i)}$$

Where X and H represent SO_3^{2-} and H^+, respectively. And the reaction B1-B6 can be summarized by two models of ii and iii:

$$A + HX + H \rightarrow Y \qquad \text{(ii)}$$

$$HX + Y \rightarrow 3H \qquad \text{(iii)}$$

Where A is BrO_3^- and Y represents one or more intermediates such as $HBrO_2$, HOBr, and Br_2. The presence of H takes into account in the participation of hydrogen ion at B7 and B8 reactions. In fact B, Q and P correspond to ferrocyanide, ferricyanide, and bromide, respectively in models of iv and v.

$$Y \rightarrow P \qquad \text{(iv)}$$

$$B + H \rightarrow Q \qquad \text{(v)}$$

If the reaction (iv) is fast enough, the system will oscillate without step (v). And if the constant rate of the reaction (v) is sufficiently high, the reaction step of (ii-iv) can be merged into the single reaction step vi.

$$A + HX + H \rightarrow nH \quad n \geq 2 \qquad \text{(vi)}$$

The Y is eliminated as a variable.

In this condition, model behaves like a clock reaction, in certain time there is a sudden increasing and exponential decrease in H^+ value. Bistability and oscillation will be obtained under flow conditions. The model can easily be adapted to describe a wide variety of pH oscillators, including iodate-sulfitethiourea (Rabai et al., 1987), iodate-sulfite-thiosulfate (Rabai and Beck, 1988), periodate-thiosulfate (Rabai et al., 1989a), periodate-hydroxylamine (Rabai and Epstein, 1989), and iodate-hydroxylamine (Rabai and Epstein, 1990)[68].

2. Result and discussion

Figure 26 demonstrates the setup of the system. We have performed a BSF oscillation reaction under the CSTR reactor. In fact, we obtained pH oscillation from the BSF system in the CSTR condition.

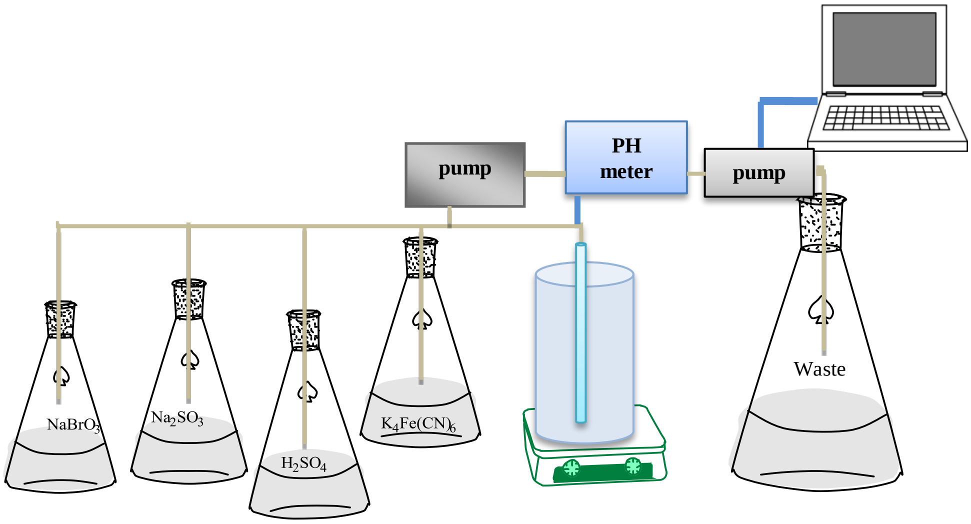

Figure 26. Experimental setup showing the CSTR, reagent sources, and the pumps.

Regular pH oscillation depends on many factors such as the flow rate of the pump, temperature, concentration of the reagents, volume of the main reactor, and speed of the magnet stirrer. In addition, the oscillation period can be changed if the concentration of the bromate solution is modified from 0.4 M to 0.8 M[64].

Epstein et al. obtained pH oscillation in a BSF system so that the oscillation period and flow rate were 20 min and 1.45×10^{-3} S^{-1} respectively. Nevertheless, we tested a BSF system using similar conditions (such as the concentration of solutions and flow rate of the pump), but the pH oscillation was unsuccessful. The pH oscillation was obtained once we utilized more concentrated solutions and increased the flow rate.

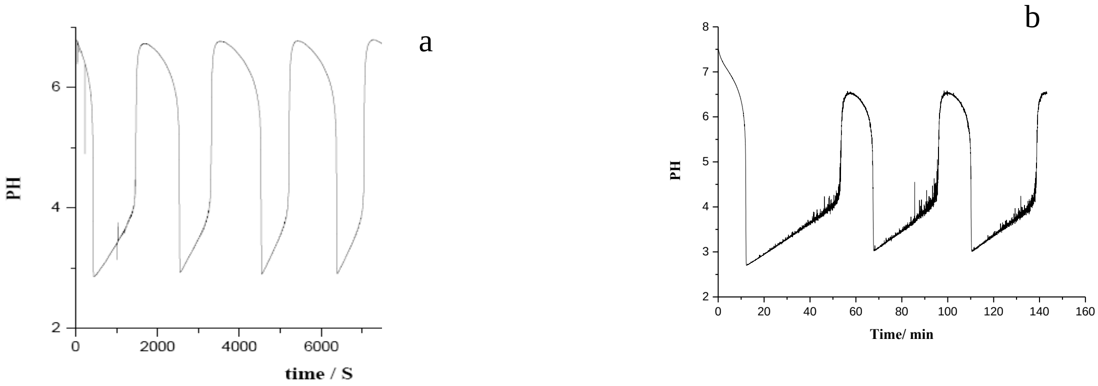

Figure 27. pH oscillation measurements in BSF system at room temperature and flow rate of a) 2 mL/min and b) 1 mL/min.

This BSF system can be combined with pH-sensitive materials such a hydrogel polymer and Cowpea Chlorotic Mottle Virus (CCMV) in order to study the effect of the pH oscillation on their dynamic behavior. According to Figure 28, hydrophilic poly(methacrylic acid)-b-poly(ethylene glycol)-b-poly(methacrylic acid) (PMAA-b-PEG-b-PMAA) triblock copolymers have different behaviors at different pHs[69]. The pH has a significant effect on the micellization behavior of this block copolymer.

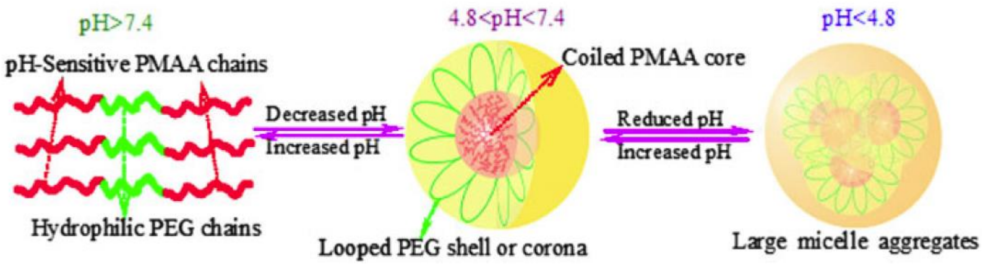

Figure 28. Represents of a pH-response triblock copolymer micelle in aqueous media with various pH values[69].

The different behaviors of the block copolymer at different pHs has been already studied, where the block copolymer was placed at the basic, acidic, and natural solutions separately. But we aim to combine the block copolymer with the BSF system while the pH oscillates continuously. Such a combined system will allow us to study the dynamic behavior of the copolymer and eventually compare it with the non-dynamic behavior.

We were able to obtain stable pH oscillation from the BSF system. We mentioned that the BSF system can be combined with a wide range of pH sensitive materials in order to study the effect of different pH on their dynamic behavior.

Coupling the pH oscillatory of a living system to other systems can create new pH oscillator systems with complex oscillation, which can help to better understand the mechanism and the dynamic behavior of such coupled systems. The gained understanding here can lead to important potential applications such as artificial muscles[70,71], controlled drug delivery systems[72], and DNA-based nanodevices[73].

3. Conclusion

In this work, we have presented the pH oscillation system that can be obtained from a BSF system, and we studied the influence of different factors such as concentration, flow rate, and temperature on this BSF system. Since there are already known pH-oscillator systems such as the formaldehyde-sulfite reaction[74], methylene Glycol-Sulfite-Gluconolactone (MGSG) reaction[75], and Bromate-Sulfite-Perchloric acid (BSH) reaction[64], it should be considered that the selected pH-sensitive materials must be compatible with all the reagents of the pH oscillation system. There is already a BSF system that contains different ranges of pH oscillation[76], but the BSF system that we gained was running at a different concentrations and lower flow rates. Such a stable and regular pH oscillation system can be combined with new pH-sensitive materials in order to study their dynamic behavior in the newly constructed system.

4. Experimental

All materials of potassium bromate (0.26 mol/L), sodium sulfite (0.3 mol/L), potassium ferrocyanide (0.08 mol/L), and sulfuric acid (0.04 mol/L) were used as received (Sigma-Aldrich) without further purification. The fresh solutions were separately pumped into the main reactor at a flow rate of 1 and 2 mL/min at 25 ºC temperature while constant volume is 40 mL. The concentration is divided by the number of feedstreams, assuming that all streams enter at the same rate.

The reaction runs under the nitrogen atmosphere, and the solutions must be fresh. Rate of magnet stirring must be around 1400 rpm. We were able to obtain stable pH oscillation around 2 hours and this oscillation can be also run even more than 2 hours. Therefore, such a stable system helps to study dynamic behavior of pH sensitive materials during the oscillation period.

4.1. pH meter

The pH changes in the main reactor were recorded continuously by utilizing a pH meter (JENCO MODEL 6230) held in reactor, and the pH data was recorded by a computer. The pH has oscillation between range of 2.8 and 6.5.

4.2. Peristaltic pump–minipuls 3

In our work peristaltic pump (Figure 29), which we have used, consists of series of rollers around the central axis. Plastic tubes are held against the rollers by clamps so when the central axis rotates, the tubes are alternately compressed and released.

Figure 29. A peristaltic pump

The pump is inexpensive and can pump from several reservoirs at once by four channels device and contains wide range of flow rate from 0-30 mL/min.

The Minipuls 3 is a rugged peristaltic pump with head speeds that is adjustable from 0 to 48 rpm. This peristaltic pump was used for delivering chemical fluids in 4 channel standard flow rate. Basically, the size of all tubing must be exactly the same. Eventually, desired flow rate can be reached by modifying flow rate of the pump manually based on the specific size of tubing that has been chosen. There are different types of pumps available.

References

1. Latthe, S. S., Gurav, A. B., Maruti, C. S. & Vhatkar, R. S. Recent Progress in Preparation of Superhydrophobic Surfaces : A Review. *Surf. Eng. Mater. Adv. Technol.* **2,** 76–94 (2012).

2. Yamanaka, M., Sada, K., Miyata, M., Hanabusa, K. & Nakano, K. Construction of superhydrophobic surfaces by fibrous aggregation of perfluoroalkyl chain-containing organogelators. *Chem. Commun.* 2248–50 (2006).

3. Feng, L. *et al.* Super-Hydrophobic Surfaces: From Natural to Artificial. *Adv. Mater.* **14,** 1857–1860 (2002).

4. Francisco, R. De *et al.* Multipurpose Ultra and Superhydrophobic Surfaces Based on Oligodimethylsiloxane-Modi fi ed Nanosilica. *ACS Appl. Mater. Interfaces* **6,** 18998–1910 (2014).

5. Wisniak, J. Anselme Payen. *Educ. Química* **16,** 578–579 (2004).

6. Krässig, H. A. *Cellulose: Structure, accessibility, and reactivity*. *Cellulose* (Copyright c 1993 Gordon and Breach Science, 1992).

7. Miljkovic, M. *Carbohydrates: Synthesis, Mechanisms, and Stereoelectronic Effects*. 560 (Springer Science & Business Media, 2009).

8. Kondo, T. The Relationship between Intramolecular Hydrogen Bonds and Certain Physical Properties of Regioselectively Substitued Cellulose Derivatives. **35,** 717–723 (1997).

9. Medronho, B., Romano, A., Miguel, M. G., Stigsson, L. & Lindman, B. Rationalizing cellulose (in)solubility: reviewing basic physicochemical aspects and role of hydrophobic interactions. *Cellulose* **19,** 581–587 (2012).

10. Wuestenberg, T. *Cellulose and Cellulose Derivatives in the Food Industry: Fundamentals and Applications*. 127 (Wiley, 2014).

11. Owusu-Apenten, R. *Introduction to Food Chemistry*. 108 (CRC Press, 2004).

12. O'sullivan, A. C. Cellulose: the structure slowly unravels. *Cellulose* **4,** 173–207 (1997).

13. Moon, R. J., Martini, A., Nairn, J., Simonsen, J. & Youngblood, J. *Cellulose nanomaterials review: structure, properties and nanocomposites. Chem. Soc. Rev.* **40,** 3941–94 (2011).

14. Imai, T., Putaux, J.-L. & Sugiyama, J. Geometric phase analysis of lattice images from algal cellulose microfibrils. *Polymer (Guildf).* **44,** 1871–1879 (2003).

15. Sugiyama, J., Vuong, R. & Chanzy, H. Electron diffraction study on the two crystalline phases occurring in native cellulose from an algal cell wall. *Macromolecules* **24,** 4168–4175 (1991).

16. Klemm, D., Philipp, B., Heinze, T., Heinze, U. & Wagenknecht, W. *Comprehensive Cellulose Chemistry, Comprehensive Cellulose Chemistry: Fundamentals and Analytical Methods*. 282 (1998).

17. Moon, R. J., Martini, A., Nairn, J., Simonsen, J. & Youngblood, J. Cellulose nanomaterials review: structure, properties and nanocomposites. *Chem. Soc. Rev.* **40,** 3941–94 (2011).

18. Siró, I. & Plackett, D. Microfibrillated cellulose and new nanocomposite materials: a review. *Cellulose* **17,** 459–494 (2010).

19. Araki, J., Wada, M., Kuga, S. & Okano, T. Flow properties of microcrystalline cellulose suspension prepared by acid treatment of native cellulose. *Colloids Surfaces A Physicochem. Eng. Asp.* **142,** 75–82 (1998).

20. Majoinen, J. *et al.* Polyelectrolyte brushes grafted from cellulose nanocrystals using Cu-mediated surface-initiated controlled radical polymerization. *Biomacromolecules* **12,** 2997–3006 (2011).

21. Kim, J. *et al.* Dispersion of cellulose crystallites by nonionic surfactants in a hydrophobic polymer matrix. *Polym. Eng. Sci.* **49,** 2054–2061 (2009).

22. Rojas, O. J., Montero, G. A. & Habibi, Y. Electrospun nanocomposites from polystyrene loaded with cellulose nanowhiskers. *J. Appl. Polym. Sci.* **113,** 927–935 (2009).

23. Wang, Z.-M., Li, L., Xiao, K.-J. & Wu, J.-Y. Homogeneous sulfation of bagasse cellulose in an ionic liquid and anticoagulation activity. *Bioresour. Technol.* **100,** 1687–90 (2009).

24. Andresen, M. *et al.* Nonleaching antimicrobial films prepared from surface-modified microfibrillated cellulose. *Biomacromolecules* **8,** 2149–55 (2007).

25. Vaca-Garcia, C., Thiebaud, S., Borredon, M. E. & Gozzelino, G. Cellulose esterification with fatty acids and acetic anhydride in lithium chloride/N,N-dimethylacetamide medium. *J. Am. Oil Chem. Soc.* **75,** 315–319 (1998).

26. Liu, G. & Zhang, G. Periodic swelling and collapse of polyelectrolyte brushes driven by chemical oscillation. *J. Phys. Chem. B* **112,** 10137–41 (2008).

27. Tedder, J. A. I. The use of trifluoroacetic anhydride and related compounds in organic synthesis. *Chem. Rev.* **55,** 787–827 (1955).

28. Heinze, T., Liebert, T. & Koschella, A. *Esterification of polysaccharides*. *Zhurnal Eksp. i Teor. Fiz.* 1–232 (Springer, 2006).

29. E. J. Bourne, M. Stacey, J. C. Tatlow, J. M. T. Studies on Trifluoroacetic Acid. Part I. Trifluoroacetic Anhydride as a Promoter of Ester Formation between Hydroxy-compounds and Carboxylic Acids. *J. Chem. Soc.* 2976–2979 (1949).

30. Maim, C. J., Mench, J. W., Kendall, D. L. & Hiatt, G. D. Aliphatic Acid Esters of Cellulose. Preparation by Acid-Chloride-Pyridine Procedure. *Ind. Eng. Chem.* **43,** 684–688 (1951).

31. Sircar, A. K., King, W. D. & Conrad, C. M. Supramolecular structure of propionylated cotton cellulose. *J. Appl. Polym. Sci.* **11,** 1951–1962 (1967).

32. Feng, L. *et al.* Super-Hydrophobic Surfaces: From Natural to Artificial. *Adv. Mater.* **14,** 1857–1860 (2002).

33. Deng, X., Mammen, L., Butt, H.-J. & Vollmer, D. Candle soot as a template for a transparent robust superamphiphobic coating. *Science* **335,** 67–70 (2012).

34. Genzer, J. & Efimenko, K. Creating long-lived superhydrophobic polymer surfaces through mechanically assembled monolayers. *Science* **290,** 2130–3 (2000).

35. Ling, X. Y., Phang, I. Y., Vancso, G. J., Huskens, J. & Reinhoudt, D. N. Stable and transparent superhydrophobic nanoparticle films. *Langmuir* **25,** 3260–3 (2009).

36. Song, J. & Rojas, O. J. Approaching super-hydrophobicity from cellulosic materials : A Review. *Nord. Pulp Pap. Res. J.* **28,** 216–238 (2013).

37. Kasai, W., Kuga, S., Magoshi, J. & Kondo, T. Compression behavior of Langmuir-Blodgett monolayers of regioselectively substituted cellulose ethers with long alkyl side chains. *Langmuir* **21,** 2323–9 (2005).

38. Cunha, A. G. *et al.* Highly hydrophobic biopolymers prepared by the surface pentafluorobenzoylation of cellulose substrates. *Biomacromolecules* **8,** 1347–52 (2007).

39. Abdelmouleh, M., Boufi, S., Salah, A., Belgacem, M. N. & Gandini, A. Interaction of Silane Coupling Agents with Cellulose. *Langmuir* **18,** 3203–3208 (2002).

40. Carlmark, A. & Malmström, E. Atom transfer radical polymerization from cellulose fibers at ambient temperature. *J. Am. Chem. Soc.* **124,** 900–1 (2001).

41. Sealey, E., J., Samaranayake, G., Todd, G., J. & Glasser, G., W. Novel Cellulose Derivatives . IV . Preparation and Thermal Analysis of Waxy Esters of Cellulose. *J. Polym. sience* **34,** 1613–1620 (1996).

42. Tomé, L. C. *et al.* Surface hydrophobization of bacterial and vegetable cellulose fibers using ionic liquids as solvent media and catalysts. *Green Chem.* **13,** 2464–2470 (2011).

43. Hornig, S. & Heinze, T. Efficient approach to design stable water-dispersible nanoparticles of hydrophobic cellulose esters. *Biomacromolecules* **9,** 1487–92 (2008).

44. Geissler, A., Biesalski, M., Heinze, T. & Zhang, K. Formation of nanostructured cellulose stearoyl esters via nanoprecipitation. *J. Mater. Chem. A* **2,** 1107 (2014).

45. Aubry, J., Ganachaud, F., Cohen Addad, J.-P. & Cabane, B. Nanoprecipitation of polymethylmethacrylate by solvent shifting: 1. Boundaries. *Langmuir* **25,** 1970–9 (2009).

46. Schubert, S., Delaney, Jr, J. T. & Schubert, U. S. Nanoprecipitation and nanoformulation of polymers: from history to powerful possibilities beyond poly(lactic acid). *Soft Matter* **7,** 1581–1588 (2011).

47. Balu, B., Kim, J. S., Breedveld, V. & Hess, D. W. in *Contact Angle, Wettability Adhes.* **6,** 235–249 (2009).

48. Zhang, W., Lu, P., Qian, L. & Xiao, H. Fabrication of superhydrophobic paper surface via wax mixture coating. *Chem. Eng. J.* **250,** 431–436 (2014).

49. Ogihara, H., Xie, J., Okagaki, J. & Saji, T. Simple method for preparing superhydrophobic paper: spray-deposited hydrophobic silica nanoparticle coatings exhibit high water-repellency and transparency. *Langmuir* **28,** 4605–8 (2012).

50. Yang, H. & Deng, Y. Preparation and physical properties of superhydrophobic papers. *J. Colloid Interface Sci.* **325,** 588–593 (2008).

51. Arbatan, T., Zhang, L., Fang, X.-Y. & Shen, W. Cellulose nanofibers as binder for fabrication of superhydrophobic paper. *Chem. Eng. J.* **210,** 74–79 (2012).

52. Werner, O., Quan, C., Turner, C., Pettersson, B. & Wågberg, L. Properties of superhydrophobic paper treated with rapid expansion of supercritical CO2 containing a crystallizing wax. *Cellulose* **17,** 187–198 (2010).

53. Barona, D. & Amirfazli, A. Producing a superhydrophobic paper and altering its repellency through ink-jet printing. *Lab Chip* **11,** 936–40 (2011).

54. Klemm, D., Heublein, B., Fink, H.-P. & Bohn, A. Cellulose: fascinating biopolymer and sustainable raw material. *Angew. Chem. Int. Ed. Engl.* **44,** 3358–93 (2005).

55. Segal, L., Creely, J. J., Martin, A. E. & Conrad, C. M. An Empirical Method for Estimating the Degree of Crystallinity of Native Cellulose Using the X-Ray Diffractometer. *Text. Res. J.* **29,** 786–794 (1959).

56. Jandura, P., Kokta, B. V & Riedl, B. Fibrous Long-Chain Organic Acid Cellulose Esters and Their Characterization by Diffuse Reflectance FTIR Spectroscopy ,

Solid-State CP / MAS 13 C-NMR , and X-Ray Diffraction. *J. Appl. Polym. Sci.* **78,** 1354–1365 (2000).

57. Marlene *et al.* in *Nat. Bur. Stand. Monoger.* 114 (1976).

58. Sadeghifar, H., Filpponen, I., Clarke, S. P., Brougham, D. F. & Argyropoulos, D. S. Production of cellulose nanocrystals using hydrobromic acid and click reactions on their surface. *J. Mater. Sci.* **46,** 7344–7355 (2011).

59. Hornig, S., Heinze, T., Becer, C. R. & Schubert, U. S. Synthetic polymeric nanoparticles by nanoprecipitation. *J. Mater. Chem.* **19,** 3838–3840 (2009).

60. Radley, J. A. *US Pat.* **2506892,** (1950).

61. Nagel, M. C. V & Heinze, T. Study about the efficiency of esterification of cellulose under homogenous condition: dependence on the chain length and solvent. *Lenzinger berichte* **90,** 85–92 (2012).

62. Geissler, A., Loyal, F., Biesalski, M. & Zhang, K. Thermo-responsive superhydrophobic paper using nanostructured cellulose stearoyl ester. *Cellulose* **21,** 357–366 (2014).

63. Geissler, A., Chen, L., Zhang, K., Bonaccurso, E. & Biesalski, M. Superhydrophobic surfaces fabricated from nano- and microstructured cellulose stearoyl esters. *Chem. Commun. (Camb).* **49,** 4962–4 (2013).

64. Zaknoun, F., Al-ghoul, M. & Sultan, R. pH Oscillations in the Bromate-Sulfite-Perchloric Acid Reaction. *Chaotic Model. Simul.* **2,** 387–394 (2012).

65. Galas, J. & Estevez-Torres, A. A chemical oscillator in a nano-liter scale microfluidic open reactor. *16th Int. Conf. Miniaturized Syst. Chem. Life Sci. Okinawa, Japan* 608–610 (2012).

66. Krisztina, K.-C., Epstein, I. R. & Orban, M. Systematic design of chemical oscillators using complexation and precipitation equilibria. *Nature* **433,** 139–142 (2005).

67. Kovacs, K., Leda, M., Vanag, V. K. & Epstein, I. R. Small-amplitude and mixed-mode pH oscillations in the bromate-sulfite-ferrocyanide-aluminum(III) system. *J. Phys. Chem. A* **113,** 146–56 (2009).
68. Epstein, I. R. & Pojman, J. A. in *An Introd. to nonlinear Chem. Dyn. Oscil. Waves, Patterns, Chaos* 1–408 (1998).
69. Luo, Y.-L., Yu, W. & Xu, F. pH-responsive PMAA-b-PEG-b-PMAA triblock copolymer micelles for prednisone drug release and release kinetics. *Polym. Bull.* **69,** 597–620 (2012).

70. Howse, J. R. *et al.* Reciprocating power generation in a chemically driven synthetic muscle. *Nano Lett.* **6,** 73–7 (2006).

71. Yoshida, R., Tanaka, M., Onodera, S., Yamaguchi, T. & Kokufuta, E. In-Phase Synchronization of Chemical and Mechanical Oscillations in Self-Oscillating Gels. *J. Phys. Chem. A* **104,** 7549–7555 (2000).

72. Misra, G. P. & Siegel, R. a. Multipulse drug permeation across a membrane driven by a chemical pH-oscillator. *J. Control. Release* **79,** 293–7 (2002).

73. Liedl, T. & Simmel, F. C. Switching the conformation of a DNA molecule with a chemical oscillator. *Nano Lett.* **5,** 1894–8 (2005).

74. Kovacs, K., McIlwaine, R., Gannon, K., Taylor, a F. & Scott, S. K. Complex behavior in the formaldehyde-sulfite reaction. *J. Phys. Chem. A* **109,** 283–8 (2005).

75. Kovacs, K., McIlwaine, R. E., Scott, S. K. & Taylor, A. F. pH oscillations and bistability in the methylene glycol-sulfite-gluconolactone reaction. *Phys. Chem. Chem. Phys.* **9,** 3711–6 (2007).

76. Kovacs, K., Leda, M., Vanag, V. K. & Epstein, I. R. Small-amplitude and mixed-mode pH oscillations in the bromate-sulfite-ferrocyanide-aluminum(III) system. *J. Phys. Chem. A* **113,** 146–56 (2009).